Eric Siciliano Rego

Variation of minerals and clay minerals recorded in the Neo-Tethys (central Turkey): new evidence of climatic changes during the middle Eocene

Dissertação apresentada ao Instituto Oceanográfico da Universidade de São Paulo, como parte dos requisitos para obtenção do título de Mestre em Ciências, Programa de Oceanografia, área de Oceanografia Geológica

Orientador:

Prof. Dr. Luigi Jovane

São Paulo
2017

Universidade de São Paulo

Instituto Oceanográfico

Variation of minerals and clay minerals recorded in the Neo-Tethys (central Turkey): new evidence of climatic changes during the middle Eocene

Eric Siciliano Rego

Dissertação apresentada ao Instituto Oceanográfico da Universidade de São Paulo, como parte dos requisitos para obtenção do título de Mestre em Ciências, área de Oceanografia Geológica

Julgada em ____/____/____

_____	_____
Prof(a). Dr(a).	Conceito
_____	_____
Prof(a). Dr(a).	Conceito
_____	_____
Prof(a). Dr(a).	Conceito

Table of Contents

Agradecimentos

Primeiramente, gostaria de agradecer a minha família por todo suporte, não só nos últimos dois anos, mas ao longo da vida inteira. Sem eles, nada disso seria possível.

Muito obrigado, de verdade, à todos que fizeram parte dessa caminhada. Ao Prof. Luigi Jovane, que abriu as portas e me apresentou não só a oportunidade de trabalho, mas também de conhecer pessoas nessa área que mudariam minha perspectiva de vida. Quanto a isso, serei eternamente grato. Outras pessoas tiveram um papel fundamental nesses últimos tempos, como o Martino, tanto nas conversas e conselhos como nas sugestões para o trabalho. Não poderia deixar de agradecer a professora Lucy, muito obrigado por todo o tempo dedicado que fez toda a diferença para me dar confiança e seguir adiante. Daniel, parceiro de campo, de congresso e de laboratório, quantos bons momentos, muito obrigado! Um obrigado bem grande a todos do laboratório!

Gostaria de agradecer aos funcionários do IO, desde todo o pessoal da limpeza, ao pessoal da secretaria (Ana Paula, Letícia, Daniel), sempre muito atenciosos e nos ajudando da melhor maneira possível. Um obrigado especial a Lourdes e a Vera, que me deram um "abrigo," bem antes de começar o meu mestrado. Eu sou muito grato por toda a ajuda naquele período, sem vocês também não sei como teria sido.

Eu tive a sorte gigantesca de ter conhecido pessoas que ao longo do tempo se tornaram família para mim. Todo a família Geoboulder, inúmeros amigos da Geologia, Biologia e IO, que tornaram meus dias muito melhores e fizeram com que eu me sentisse em casa mesmo aqui em São Paulo. Eu acho que é muito nome para pouco espaço, mas deixo aqui escrito minha enorme gratidão pela amizade vocês.

Um obrigado especial a Malu, por toda a amizade e companheirismo, que mesmo as vezes distante, fazia parte do meu dia-a-dia, tornando-o sempre melhor.

À FAPESP, por todo apoio financeiro ao projeto de mestrado (2015/16501-4) e ao projeto BEPE (2016/02288-0).

Resumo

Minerais e argilominerais em sucessões sedimentares são excelente ferramentas para a reconstrução de condições ambientais. Dado o estado de preservação dos argilominerais, é possível identificar como eles foram formados, fornecendo informação sobre as condições de intemperismo no continente e sobre condições geoquímicas na coluna d'água. Este estudo apresenta novos dados mineralógicos da seção de Baskil, uma sucessão do Eoceno médio altamente preservada no Neo-Tethys (Turquia central). Uma mudança na assembléia mineralógica com maiores concentrações de ilita e clorita (subseção I) para um intervalo dominante de esmectita detrítica (subseção II) caracteriza uma mudança na área de fonte de rochas metamórficas para rochas ígneas e mudanças de condições de intemperismo físico para intemperismo químico. Este período coincide com o Ótimo Climático do Eoceno Médio (MECO), indicando uma assinatura mineralógica do evento. A paligorsquita autigênica teve um aumento na porção media e superior da seção, indicando condições favoráveis na coluna de água para a sua formação. Possívelmente as condições na circulação do oceano naquela região mudaram após 40 Ma, formando uma coluna de água estratificada com condições mais quentes e salinas em profundidades maiores, favorecendo precipitação de paligorsquita e dolomita. A evolução mineralógica da seção de Baskil reflete como as fontes e os regimes de intemperismo mudaram ao longo do tempo, e como essas mudanças podem estar relacionadas aos processos globais (e.g. MECO) e /ou a processos locais e regionais.

Palavras-chave: minerais, argilominerais, esmectita, paligorsquita, Neo-Tethys, MECO

Abstract

Minerals and clay minerals in continental sedimentary successions are valuable tools for reconstructing past environmental conditions. Given the state of preservation of clays minerals, it is possible to identify how they were formed, providing clues about continental weathering conditions (inherited minerals) and geochemical conditions in the water column (neoformed or transformed). This study presents new mineralogical data from the Baskil section, a highly preserved middle Eocene succession in the Neo-Tethys (central Turkey). A gradual shift from a well-crystalline illite and chlorite interval (interval I) to a detrital smectite dominant interval (interval II) characterizes a change in source area from metamorphic to igneous rocks and changes from physical to chemical weathering conditions on land. This period coincides with the Middle Eocene Climatic Optimum (MECO), indicating a mineralogical signature of the event. Higher content of terrigenous input being deposited from 40.5 to 40 Ma caused a dilution effect of the carbonate materials as calcite and dolomite significantly decreases. Authigenic palygorskite showed an increasing trend from the middle to the uppermost portion of the section, indicating favorable conditions in the water column for its formation. We assume that conditions in the ocean circulation changed after 40 Ma, forming a stratified water column with warmer and saline conditions at greater depths, favoring palygorskite and possibly authigenic dolomite precipitation. The mineralogical evolution of the Baskil section reflects how sources and weathering regimes changed through time, and how these changes can be related to global (i.e. MECO) and/or local to regional processes.

Key-words: minerals, clay minerals, smectite, palygorskite, Neo-Tethys, MECO

List of Figures

List of Tables

1.Introduction

The Earth has experienced vast periods of climatic and environmental changes throughout its history. If we look at only the Phanerozoic, going back approximately 540 Ma, a relatively small slice of time (when compared to ~ 4 Billion years ago; the planets' origin), we have seen five major extinction events, changed from a hot (greenhouse) to a cold planet (icehouse), the ocean chemistry has changed, and continents have collided to form incredibly high mountain ranges, and drifted apart opening oceans with abyssal depths. It seems, in my humble opinion, that disequilibrium has always been present in Earth's system, but at the same time, it has found its way to evolve and main life as it is today.

This ongoing evolutionary process perpetuates, and climatic and environmental changes are now being modulated by us, humans (homo sapiens), who have been around for approximately 200 kyr ago. The well-known and extensively used example is the rise in global surface temperatures. Could these past warmer geological periods have anything in common with our present, and most importantly with our near future? A recent study made by (FOSTER et al., 2017) showed that by the 23rd century climate could reach a warmth never seen in the past 420 million years. Understanding the underlying mechanism, such as causes, effects and duration of past climatic and environmental changes could potentially give us clues regarding our close warmer future.

My motivation for this study was mainly to be working on a geological period of approximately 40 Ma, in which climate was at a transition phase from greenhouse to icehouse conditions. During this cooling trend in the Eocene Epoch, a global warming event took place, which is still not well understood. My study was to look at clay minerals to try to understand environmental conditions over middle Eocene, how and what factors influenced their mineralogical changes. Were they related to climate, source rocks or

environmental conditions? Maybe a combination of all these? I hope by answering these questions we can have a better understanding of what was happening in in the past, and maybe, one day, we could know if this would happen in the future.

1.1 The origin of clay minerals: a brief overview

Clay minerals form about one-third of all present sedimentary rocks and are the most abundant minerals at the surface of the Earth (MOORE; REYNOLDS, 1997). This group of hydrous silicate minerals are composed of two-dimensional Si-bearing tetrahedral, and Al-bearing octahedral sheets stacked in a regular arrangement (FAGEL, 2007). Despite their abundancy, clays[1] are highly demanded for industrial purposes (MURRAY, 2007). Properties such as adsorption, catalysis and plasticity turned them into useful tools from the development of traditional ceramics to modern nanotechnology research (ZHOU; KEELING, 2013). Additionally, understanding clay minerals formation processes, dispersal patterns and state of preservation and/or alteration can provide valuable information regarding source areas and how past environmental conditions changed through the geological time (CHAMLEY, 1989; VELDE, 1995; MERRIMAN, 2005; MORTON, 2005; EHLMANN et al., 2011).

Clay minerals originates mostly from the alteration of pre-existing minerals, through weathering processes, which in turns initiates the "clay cycle" proposed by MERRIMAN (2005) (Figure 1). This near-surface alteration process leads to the development of soils and an array of different pedogenic profiles which will later be partially and/or entirely eroded, transported and deposited into sedimentary basins (GALÁN, 2006). Inherited clays, also known as detrital clays, are transported to the

[1] The terms clays and clay minerals will be used to refer to phyllosilicates and not the clay size fraction (<2 μm), unless stated otherwise.

sedimentary basins with no or only little modification, consequently giving information about the weathering conditions on the adjacent land-masses where they were formed (VELDE, 1995). This process usually occurs in two ways: (1) physical breakdown of parent rocks (physical weathering) and through (2) dissolution of pre-existing clays and non-clay minerals, which under normal pH conditions hydrolysis is the main component involved (chemical weathering) (CHAMLEY, 1989).

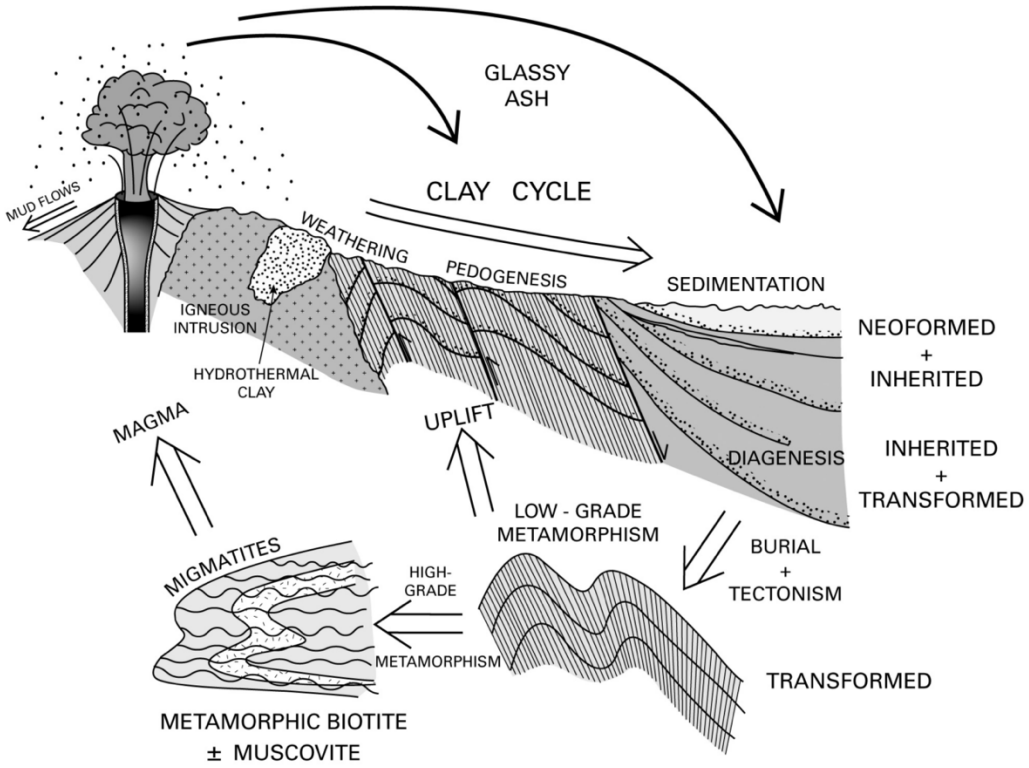

Figure 1: The clay cycle as proposed by Merriman (2005) showing different clay formation and alteration processes (MERRIMAN, 2005).

As time goes by, these deposits become thicker, and buried clays are likely to be transformed in response to geothermal conditions and/or geotectonic evolution of the basin (MERRIMAN, 2005).These clays are referred to as authigenic, which means they were formed *in situ*. Even though they are considered as a minor component of clay minerals (VELDE, 1995), they can still characterize geochemical conditions where they

originated. However, is important to mention that any sing of diagenesis[2] can mask or erase completely the climatic signal imprinted by detrital clays (SINGER, 1984; THIRY, 2000). In addition, neoformation processes occurs either from minerals precipitating from solution, given a specific environmental condition, or from crystallization of amorphous minerals (EBERL, 1984). Once the superficial or buried rocks and sediments are uplifted, the clay cycle reinitiates.

Despite climatic conditions, a combination of other factors such as parent material (rock-type), topography and time will determine which clays mineral assemblages are found in a specific continental and/or marine sedimentary succession (GALÁN, 2006). Detrital smectite formed in soils is a product of chemical weathering and it is normally associated with alteration of volcanic materials (CHAMLEY, 1989; LIU et al., 2003; LIMMER et al., 2012) under warm conditions in areas of low-lying poorly drained soils with contrasting dry and wet seasons (ROBERT; CHAMLEY, 1991; WILSON, 1998; FRANKE; EHRMANN, 2010). On the other hand, kaolinite is usually formed under warm and wet conditions with strong leaching associated to tropical regions (THIRY, 2000). Illite and chlorite are usually inherited from crystalline rocks, through alteration of muscovite and biotite, and are typically found in higher latitudes where physical weathering prevails (EHRMANN; SETTI; MARINONI, 2005; BORCHERS et al., 2011). The fibrous clay palygorskite, however, is more often neoformed or transformed in soils, shallow-marine environments, and in the deep-sea. These Mg-rich clays are characteristic of arid and semi-arid climates (e.g. Mediterranean region) when formed in soils and in shallow-marine environments (HILLIER, 1995). However, to precipitate in sediments from deep-sea locations, warmer, saline and alkaline conditions are required with

[2] The term is used to refer to "all of the changes that a sediment undergoes after deposition and before the transition to metamorphism" (MIT).

favorable Si and Mg activities (PLETSCH, 2001; GALÁN; POZO, 2011; THIRY; PLETSCH, 2011).

1.2 Clay minerals as weathering proxies

Previous studies have used the distribution and abundances of clay minerals assemblages in surface sediments from oceanic basins (BISCAYE, 1965; GRIFFIN; WINDOM; GOLDBERG, 1968; KOLLA; HENDERSON; VENKATARATHNAM; BISCAYE, 1973; BISCAYE, 1976) and the world oceans (RATEEV et al., 1969; WINDOM, 1976; RATEEV; SADCHIKOVA; SHABROVA, 2008) to establish distribution patterns related to latitudinal climate regimes, weathering conditions, wind regimes, river discharge and ocean currents (Figure 2). Higher concentrations of kaolinite are in low latitudes where there is prevailing chemical weathering under warm and humid conditions (Figure 2a). Illite and chlorite reach their maximum values in middle to low latitudes, particularly in the northern hemisphere indicating detrital origin due the large land-masses, where physical weathering dominates (Figure 2b, c). Smectite is abundant in the south Pacifc, indicating a volcanic origin (Figure 2d) (STEIN, 2016).

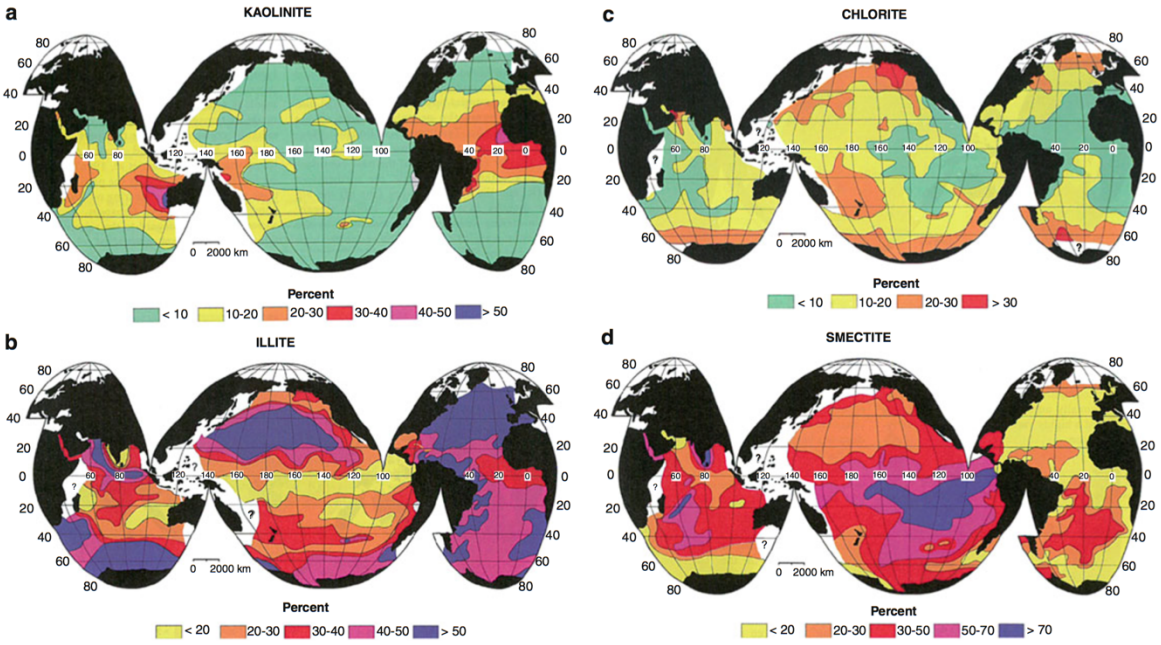

***Figure 2**:* Distribution of kaolinite (a), illite (b), chlorite (c), and smectite (d) in superficial sediments from the world ocean (after STEIN, 2016).

This relationship between clay mineral assemblages in surface sediments and modern climate conditions gave scientists the possibility to go back in the geological time through sediment cores and continental succession and infer paleoceanographic and paleoclimatic conditions (e.g. FAGEL; ROBERT; HILLAIRE-MARCEL, 1996; PETSCHICK; KUHN; GINGELE, 1996; X. GINGELE et al., 2002; EHRMANN; SETTI; MARINONI, 2005; ALIZAI et al., 2012; CHEN et al., 2016). Epochs of significant climatic changes, such as the ones observed at the beginning of the Cenozoic Era (e.g. Eocene Epoch), are ideally to test whether clays respond to such changes from a regional to a global context.

1.3 Climatic conditions during the Eocene

The Eocene epoch (56 – 38 Myr ago) was marked by a long-term cooling trend interrupted by a series of warmer transient periods (ZACHOS et al., 2001; ZACHOS;

DICKENS; ZEEBE, 2008) (Figure 3). Such climatic perturbations were typically identified by a negative carbon isotope excursion (CIE) and carbonate dissolution on the sea-floor, which included short-duration events such as the Paleocene-Eocene Thermal Maximum (PETM) (ZACHOS et al., 2005; WESTERHOLD et al., 2007) and the Early Eocene hyperthermals (LOURENS et al., 2005; GALEOTTI et al., 2010; SEXTON et al., 2011; COCCIONI et al., 2012; WESTERHOLD; RÖHL; LASKAR, 2012). Additionally, longer-duration events like the early Eocene Climatic Optimum (EECO) and the still enigmatic middle Eocene Climatic Optimum (MECO) (BOHATY; ZACHOS, 2003; BOHATY et al., 2009; SLUIJS et al., 2013) left their imprints in continental and oceanic sedimentary successions.

Earth's climate is changing towards warmer conditions that are similar to other warmer periods in Earth history, such as during the Eocene, which have been identified using various proxies, including specific mineral assemblages (ROBERT; KENNET, 1994; WANG et al., 2011; BORNEMANN et al., 2014; PUJALTE; BACETA; SCHMITZ, 2015; KEMP et al., 2016). Stratigraphic changes in clay mineral suites are a valuable tool for the reconstruction of environmental history on global to regional scales (VELDE, 1995; CHEN; LIU; KISSEL, 2017). Provided that the diagenesis has not erased the climate signal and only detrital clay minerals are present, these are reliable minerals for paleoenvironmental reconstructions (THIRY, 2000), and additionally can indicate potential source areas and infer oceanic circulation patterns (e.g. FAGEL; ROBERT; HILLAIRE-MARCEL, 1996; PETSCHICK; KUHN; GINGELE, 1996; X. GINGELE et al., 2002).

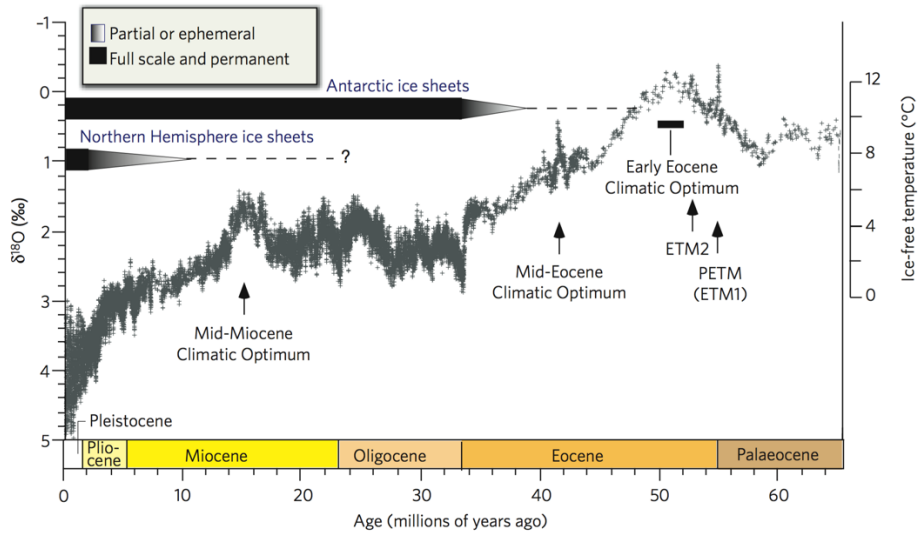

Figure 3: A compiled data set of stable oxygen isotopes from benthic foraminifera showing a cooling trend from 65 Ma until present, highlighting warming periods throughout the globe (after ZACHOS et al., 2008).

This study characterizes the minerals and clay mineral assemblages from a well-preserved Neo-Tethys succession in central Turkey, which expands through the middle Eocene. We test the hypothesis that variations in clay minerals reflect potential terrestrial source areas and climatic conditions. In addition, we relate changes in the clay mineral assemblages to the terrestrial environmental conditions resulting from global warming during the MECO warming period, for which only a few studies exist (BOSBOOM; GUO, 2014; METHNER et al., 2016).

1.4 Hypothesis

Previous studies, as mentioned above, have shown that depending on climate and environmental conditions a specific group of clay minerals can be formed. During warmer intervals, smectite and kaolinite are often observed as product of chemical weathering, while illite and chlorite are characteristic of colder intervals due to physical weathering. Since we are studying a period in which global temperatures rose, our hypothesis is based on an increase of smectite and/or kaolinite during the warming phase (product of chemical

weathering) and increase in illite and chlorite during cold phase (product of physical). Source rocks also influence the mineralogy and consideration regarding the geology of the Elazig basin is taken in combination with climatic and environmental conditions.

2. Objectives

Characterize the mineralogical assemblages from a terrestrial succession in central Turkey through X-Ray Diffraction (XRD) and Scanning Electron Microscopy (SEM) in order to obtain information on potential source areas and on prevailing paleoenvironmental conditions during the middle Eocene.

2.1 Specific Objectives

a.) Determine the bulk and clay mineralogy for the studied succession through a semi-quantitative method;

b.) Correlate minerals and clay minerals with actual and potential source rocks to infer their origin and changes in sources through the studied interval;

c.) Analyze selected samples through SEM to determine if minerals are characteristic of a detrital or authigenic formation;

d.) Correlate trends of minerals and clay minerals' relative abundancy with a global warming period and identify possible environmental conditions during their time of deposition

3. Geological Context (Study Area)

The studied stratigraphic succession, the Baskil section, occurs in central Turkey and is part of the Kırkgeçit Formation, in the Elazığ basin, 19.8 km NW of the town of Baskil (located at 38°36'30.34''N, 38°36'03.46''E) (Figure 4). This section

measures 357 msl (stratigraphic meters from the base of the section) with a paleodepth of ~300-600 m (RODELLI et al., in 2017), which is composed mainly of thick-bedded to massive hemipelagic marlstone, formed by a mix of carbonate with fine-grained clastic rock (DONOVAN; PICKERILL, 2013), intercalated with calcarenite beds. Accumulation of large benthic foraminifera (LBF) within the calcarenite beds, which range from 15 cm to ~1 m thick, has been previously reported (ÖZCAN et al., 2006). The age model for the Baskil section was presented by RODELLI et al. (2017), and extends from 41.7 to 37.2 Ma.

The Kırkgeçit Formation (dark grey portion of the map on Figure 4) has an E–W oriented area of approximately 40 km wide and 100 km long, which consists of clastic deep-water and shelf deposits fed from a subaerially-exposed hinterland (ÖZKUL; KEREY, 1996; CRONIN et al., 2000). These hemipelagic sediments are interpreted to be deposited in a back-arc basin on continental crust (CRONIN et al., 2007; ÇELIK, 2013). Furthermore, within the Kırkgeçit Formation, the Baskil section has not been deformed and does not show alteration despite the regional active tectonic regime. The good state of preservation of the section makes this location a primary target to develop proxies for paleoclimatic, paleoceanographic, and biotic events (RODELLI et al., 2017).

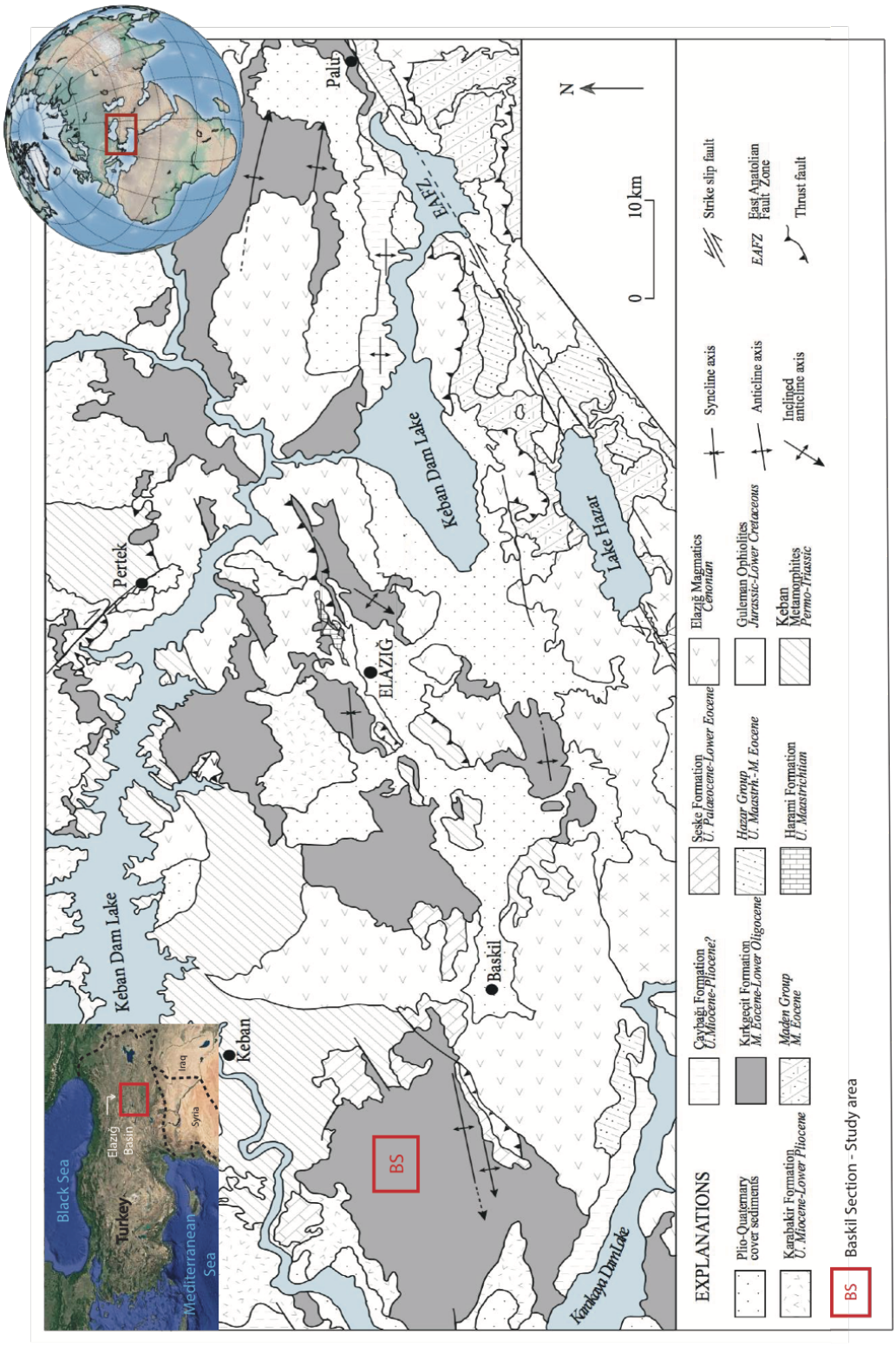

Figure 4*:* Geological map of the Elazığ basin, showing in gray the middle Eocene deposits from the Kırkgeçit Formation and the location of the Baskil section (modified after ÇELIK, 2013).

The basement units for the Cenozoic sediments in the Elazığ basin are the Permo-Triassic Keban metamorphic rocks and the Late Cretaceous (Cenomanian) Elazığ

Magmatic rocks (AKSOY; TÜRKMEN; TURAN, 2005). The former consists of marble, calc-phyllite, calc-schist, and metaconglomerate, which have undergone amphibolite- to greenschist-facies metamorphism and was thrust over younger formations (TURAN; BINGÖL, 1991) the latter is made up of basalt, andesite, pillow lava, dacite, aplite, dolerite, and plutonic rocks (BINGÖL; BEYARSLAN, 1996). Both units could have been potential source areas for the mineralogical assemblage found in the studied section. Overlaying the magmatic rocks is the Harami Formation, composed of late Campanian–Maastrichtian carbonate build-ups. Mass-flow conglomerates make up of Permo-Triassic Keban Metamorphic rocks and Late Cretaceous magmatic rock pebbles (AKSOY; TÜRKMEN; TURAN, 2005) compose the early Paleocene deposits in the basin. The Kuşçular and Seske Formations (late Paleocene – early Eocene) are stratigraphically located at the base as a sandy limestone grading up into pure limestone composed mainly of algae and benthic foraminifera, with a high fraction of micritic matrix (AKSOY; TÜRKMEN; TURAN, 2005).

4. Material and Methods

4.1 Field Sampling

Two field trips were made to central Turkey, the last one being in June of 2015, where samples were collected. An initial lithostratigraphic log was defined and the sedimentary succession was measured (Figure 5). Afterwards, samples were taken to the Istanbul Technical University (ITU), where they were cut and latter brought to Brazil.

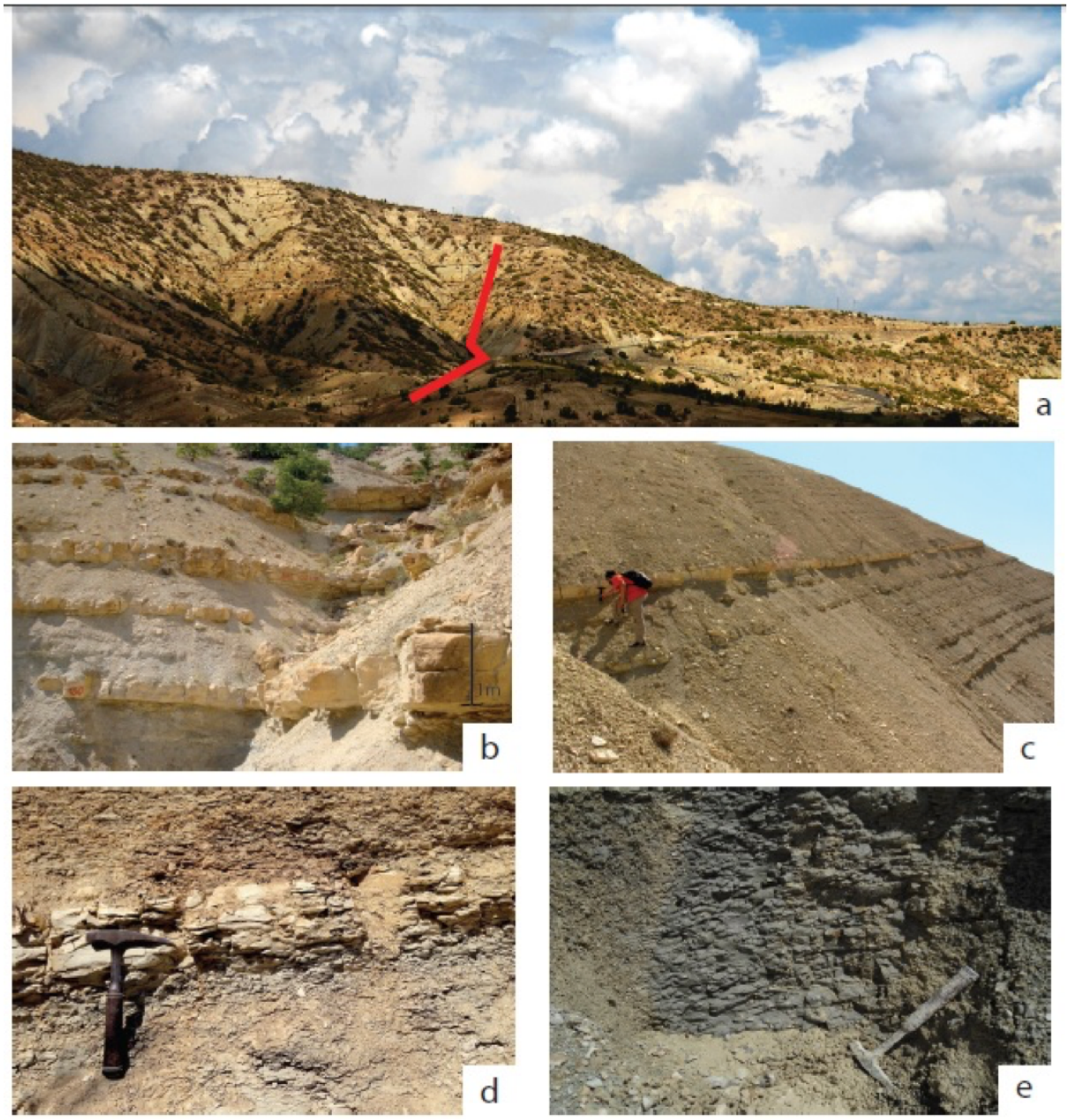

***Figure 5**:* a) panoramic view of the studied section, highlighted with a red line; b) view of 1 meter thick calcarenites; c) intercalation of several thin calcarenites in the marlstone, the thickest is at 106 msl; d) detail of a calcarenite about 20 cm thick in the lower part of the section; e) detail of pristine gray marl under the detrital covering.

4.1.1 Lithostratigraphy

A specific portion of the section, from 180 to 200 meters, was analyzed in closer detail mainly due to six strata, here named Sisters (1-6), which called the attention due to their thickness and location along the section. Facies description were performed

along with thickness measurements from each layer and sampling for specific thin-section observation.

4.2 X-ray diffraction (XRD)

X-ray diffraction has been widely used to obtain information about structures of crystalline materials. Normally, a powdered material is exposed to a monochromatic beam of X-ray, which will in turn interfere or diffract when the beam hits the crystal lattice. The diffraction angles will vary with the distance (d-spacing) between adjacent planes of atoms in the crystal. Subsequently, a distinctive diffraction pattern is generated for every crystalline material (e.g. minerals). These diffraction angles can be used to calculate the d-space (d) according to Bragg's Law:

$$\lambda = 2dsin\theta \qquad (4.1)$$

The wavelength of the incident beam (λ) is usually fixed for most diffractometers, and θ represents the angle between the diffracted beam and the crystallographic plane (MCREYNOLDS; SKAGGS; SCHROEDER, 2008). For example, each mineral having its own crystalline structure, will have a different set of diffraction peaks based on their planes of atoms (Figure 6). Finally, by knowing the d-spacing and the diffracted patterns, it is possible to perform mineral identification based on comparison with standard materials. This technique was applied in this study to identify minerals and clay minerals from marlstone samples.

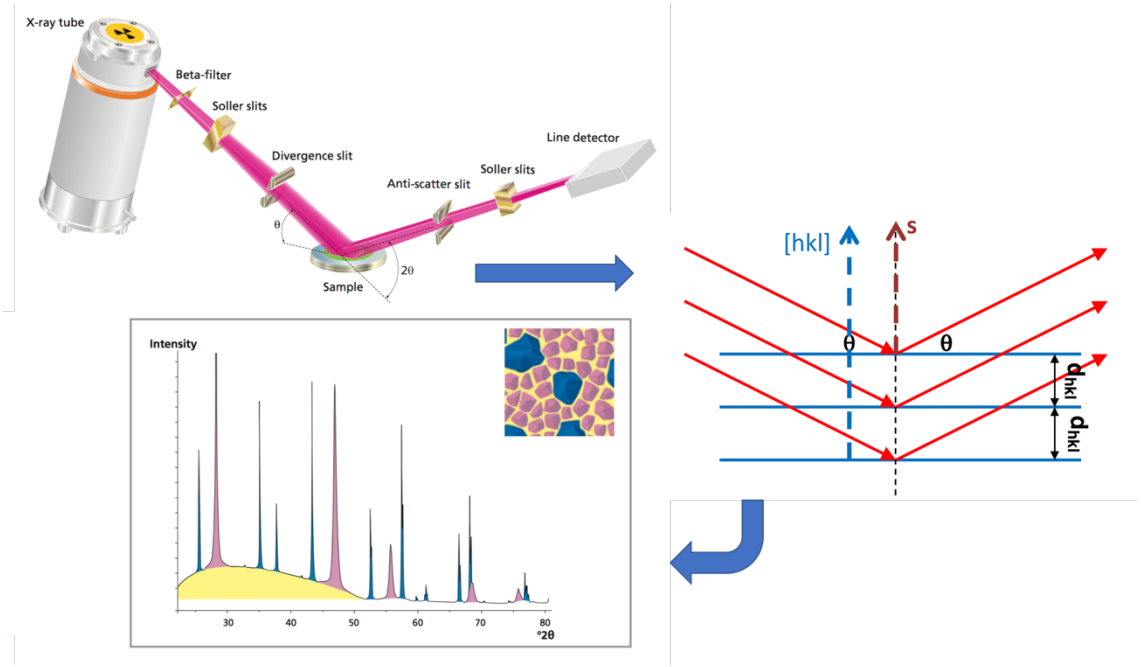

***Figure 6**:* Representative sketch of incident X-rays being emitted (tube) and received (detector) and an example of x-rays (red arrows) diffracting from parallel atomic planes (blue line) at a specific angle (theta). Diffractogram generated after the diffraction process showing distinct crystalline structures with different peaks and a hump representing amorphous material. (modified sketch taken from Panalytical).

4.3 Mineralogical Analyses

A total of one hundred and twenty samples of marlstones from the Baskil Section were analyzed using XRD for the bulk fraction and sixty-nine samples for the clay size (<2 μm) fraction. Measurements were made using a Panalytical X'Pert^3 Pro diffractometer with an X'celerator detector (Cu*K*α radiation; 45 kV; 40mA) at the United States Geological Survey (USGS), Santa Cruz, CA. The bulk and clay size fraction scanning ranges were from 3 – 70° 2θ and 3 – 30° 2θ, respectively, both with a step size of 0.03° 2θ and a measuring time of 80 seconds per step. Data processing was made with the MacDiff 4.2.5 software (PETSCHICK, 2001).

4.3.1 Bulk fraction

Bulk rock samples were powdered with a microdrill and placed in an aluminum sample holder, applying gentle pressure to allow randomly oriented aggregates. All

samples are required to have the same particle size to avoid discrepancies between minerals intensities, which could influence the semi-quantitative results. XRD patterns from randomly oriented mounts were semi-quantified according to HILLIER (2003) and MOORE; REYNOLDS (1997) using the integrated peak areas (IPA) of individual peaks by applying the following reference intensity ratios (RIR): quartz (4.26 Å) – RIR 0.91; albite (3.18 Å) – RIR 2.2; K-feldspar (3.24 Å) – RIR 1; phyllosilicates (4.5 Å) – RIR 0.71; calcite (3.03 Å) – RIR 3.1; dolomite (2.88 Å) – RIR 2.7. The IPA for each mineral identified in every diffractogram was divided by their respective RIR to be semi-quantified in such manner:

$$\text{Mineral weight (\%)} = 100^* \text{ (IPA/RIR)/sum} \qquad (2)$$

Mineral standards were used to test the XRD accuracy in relation to the RIR values and errors were calculated to be in the range of $\pm$ 5% from the known amounts as shown in Table 1.

Table 1: Mixtures of standard minerals with specific known values were made and calculated. An error of approximately $\pm$ 5% was observed between known and calculated values.

	Mineral	Integrated Peak Area (cps)	d-spacing (Å)	RIR	Known Values (%)	Calculated Values (%)
Sample 1	Calcite	109210	3.03	3.1	20	20.124
	Quartz	20773	4.26	0.91	10	13.049
	Albite	257415	3.18	2.2	70	66.837
Sample 2	Calcite	168208	3.03	3.1	50	46.234
	Quartz	49773	4.26	0.91	40	46.605
	Albite	18490	3.18	2.2	10	7.161
Sample 3	Calcite	430497	3.03	3.1	90	92.219
	Quartz	5545	4.26	0.91	3	4.046
	Albite	12372	3.18	2.2	7	3.734
Sample 4	Calcite	79180	3.03	3.1	20	19.42

	Quartz	79575	4.26	0.91	70	66.49
	Corundum	18532	2.08	1	10	14.09
Sample 5	Calcite	30078	3.03	3.1	10	5.464
	Quartz	152757	4.26	0.91	90	94.536

4.3.2 Clay size fraction

The first step required to analyze clay minerals is to remove all organic matter and calcium carbonate from the samples and afterwards separate the clay fraction (<2 μm) from the bulk material (Table 4, Sup. Material). Not only clay minerals are found in the clay fraction, however, they are more easily identified and quantified when separated from the whole-rock. All clay mineral samples followed specific treatments described by (HEIN; SCHOLL; GUTMACHER, 1976; HEIN et al., 2003). Approximately 10 g of material were soaked in a combination of 30% H_2O_2 and Morgan's solution (sodium acetate and glacial acidic acid) to remove organic matter and carbonates, respectively (Figure 7A). After the removal of organic matter and calcium carbonate, a first run in the centrifuged (2500 rpm for 5 minutes) was performed to separate the H_2O_2 and Morgan's solution from the rest of the material (Figure 7B). The following step was to wash the samples with 2% sodium carbonate (Na_2CO_3). A magnetic stirred was used to suspend again the material, which was later re-concentrated into a test tube using a 0.01% Na_2CO_3 to rinse any residues (Figure 7C). This material, which was suspended in the test tube went for a second run on the centrifuge (850 rpm for 3 minutes) (Figure 7D). After centrifugation, all material still in suspension had a settling diameter of 2 μm or less (Figure 7E).

The < 2 μm fraction was saved, and this process was repeated 10 times for every sample: re-suspending the material with 0.01% Na_2CO_3 and centrifuging the material

until all the clay size fraction was extracted from every sample (Figure 7F and G). The clay fraction was concentrated at the bottom of the best tube through another run of the centrifuge (2500 rpm for 5 minutes) and washed two times with distilled water to remove excess salts. Finally, the clay-sized fraction was oriented on zero background holders prior to analyses (Figure 7H). A complete list (a step-by-step) with specific details regarding sample preparation follows attached at the supplementary material.

A set of three diffraction patterns were made for each sample, followed by air drying (AD), ethylene glycol solvation for 24h (EG) and heating to 375°C for 1h (H), and used for mineral identification and quantification purposes. Semi-quantitative estimations for the clay mineral abundances were based on the EG curve on specific integrated peak areas of individual peaks and weighting factors, following (BISCAYE, 1965). Peak deconvolution of peak doublets was performed for the following minerals: smectite/chlorite (17/14 Å), palygorskite/illite (10.5/10 Å) and kaolinite/chlorite (3.58/3.54 Å) (GUO; UNDERWOOD, 2011; EHRMANN et al., 2015). The same weighting factors used for kaolinite and chlorite was used for palygorskite (EHRMANN et al., 2015). Clay mineral ratios were calculated from mineral relative abundances.

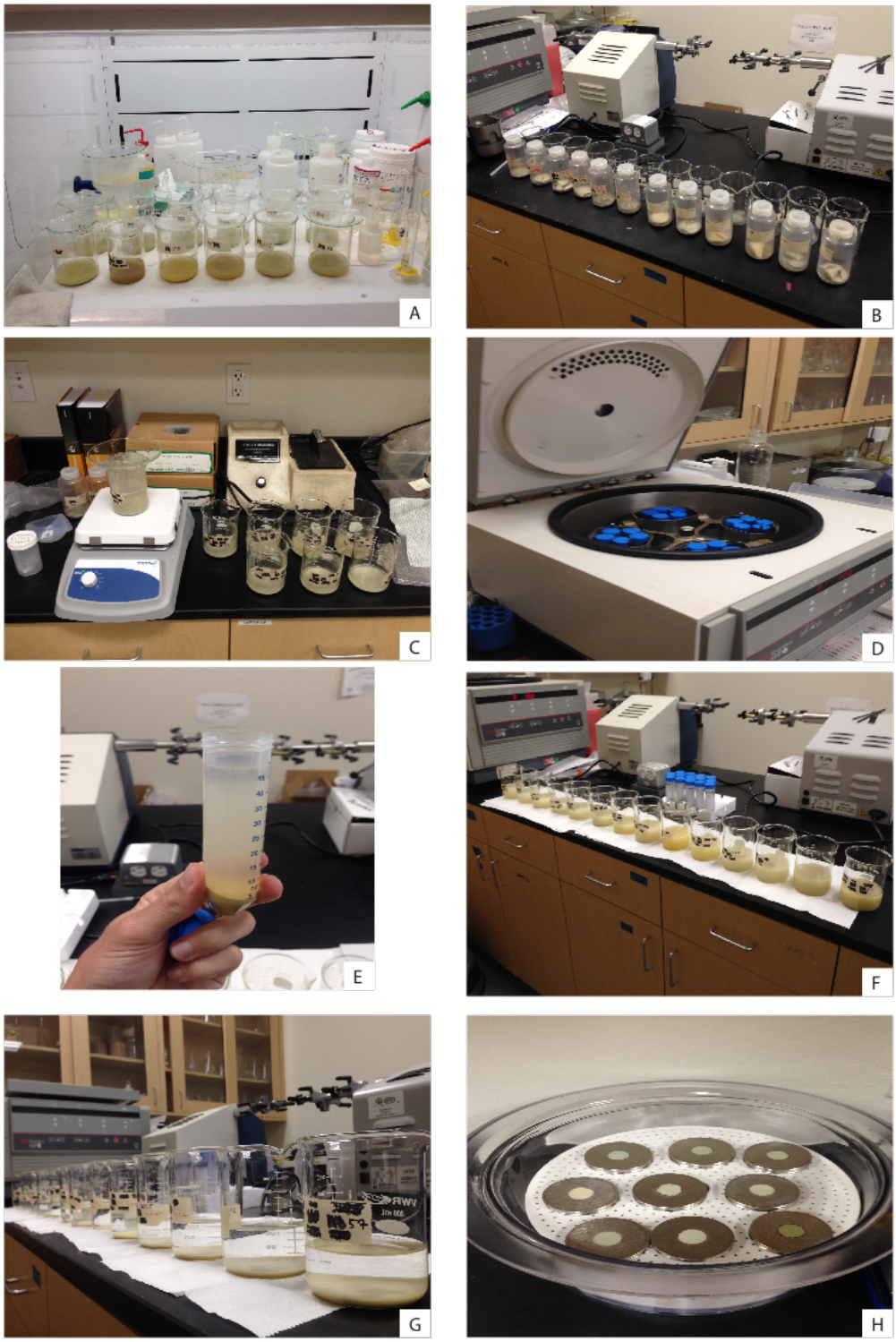

Figure 7: Pictures of sample preparation process for clay mineral analysis, showing (A) removal of organic matter and calcium carbonate, (B) separation of material through a first run in the centrifuge, (C) magnetic stirrer used with sodium carbonates, (D) centrifuge with samples prior to the analyses, (E) less than 2 µm fractionin the test tube, (F) clays (<2µm) still in suspension, (G) clays(<2µm) settled in the bottom of beakers, and samples already oriented on zero background holders prior to analisis.

Illite crystallinity was measured using the full width at half maximum height (FWHM) and the integral breadth (I Breadth) of the 001 basal illite peak on EG samples as values of Δ2°θ (Figure 8). Both measurements presented the same trends and only the FWHM will be further discussed (ALIZAI et al., 2012; LIMMER et al., 2012). Low values indicate good crystallinity (lower weathering intensity), whereas high values indicate poor crystallinity (higher weathering intensity) (LAMY; HEBBELN; WEFER, 1998; PANDARINATH, 2009). The illite chemistry was obtained from peak area ratios of the basal 002/001 (5 Å/ 10 Å) peaks. Ratios > 0.4 correspond to Al-rich illites (muscovite), while ratios < 0.15 are related to Mg and Fe-rich illites (biotite) (ESQUEVIN, 1969).

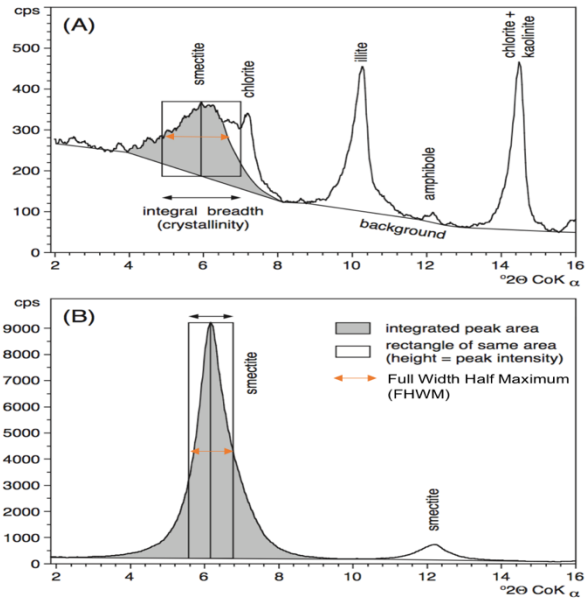

Figure 8:Measuremts used for crystallinity: integral breadth and FWHM. (A) Poorly crystallized smectite and (B) well crystalized smectite. Integrated peak area showed in grey. (modified after EHRMANN et al, 2005)

4.4 Benchtop X-ray (BTX) diffraction system

The Olympus BTX II Benchtop XRD was derived by the Mars Science Laboratory and is an ideal equipment to perform general characterization of specific crystalline materials in the field and in the laboratory. This equipment has been used in

extraterrestrial missions (e.g. Gale Crater in Mars within the Curiosity Rover) and it is now available for students at the Oceanographic Institute (IO-USP) (SARRAZIN et al., 2005; BLAKE et al., 2012).

Key features for the BTX include a vibrating sample holder, which allow samples to be analyzed in a non-oriented manner, particularly well-suited for bulk mineralogy. This equipment was previously used in paleoclimatic studies (e.g. SAVIAN et al., 2014, 2016), however a method is still under development to accomplish solely clay minerals analysis in an oriented manner. For this reason, we chose to perform our analysis using the Panalytical X'pert 3, even though more than 300 samples were analyzed with the BTX. A couple of additional results concerning the BTX will be attached in the supplementary material (Fig. 24, 25).

4.5 Scanning electron microscopy (SEM)

Small blocks of selected marlstones samples were broken to expose a fresh fracture surface representative of the texture and structure of the rock (KELLER; REYNOLDS; INOUE, 1986). Samples were coated with Au-Pd and analyzed in a TESCAN VEGA3 microscope (15kV and 10nA for imaging), which included X-ray energy dispersive spectroscopy (EDS) using an Oxford Xmax 50 detector (20 s of live counting time). All the data were refined with the AZtech software and processed at the USGS, Menlo Park, CA. Additional samples were analyzed at the Institute of Geosciences (IGc), at the University of São Paulo, Brazil, where a LEO-440i scanning electron microscope coupled with an energy dispersive spectrometer (EDS) was used, and samples coated with carbon.

5. Results

5.1 Lithostratigraphy

The most significant lithological changes in the Baskil section are generally marlstones intercalated with calcarenite beds throughout the entire interval. Calcarenite beds had a range of ~20 cm to 1 m thick and were less frequently observed from 0 to 180 m. After this interval, from 180 to 200 m, six strata (Sisters 1-6) in close proximity to each other show distinct lithological changes (Figure 9). Through the upper portion of the section, after the Sisters' interval, calcarenite beds were observed more frequently.

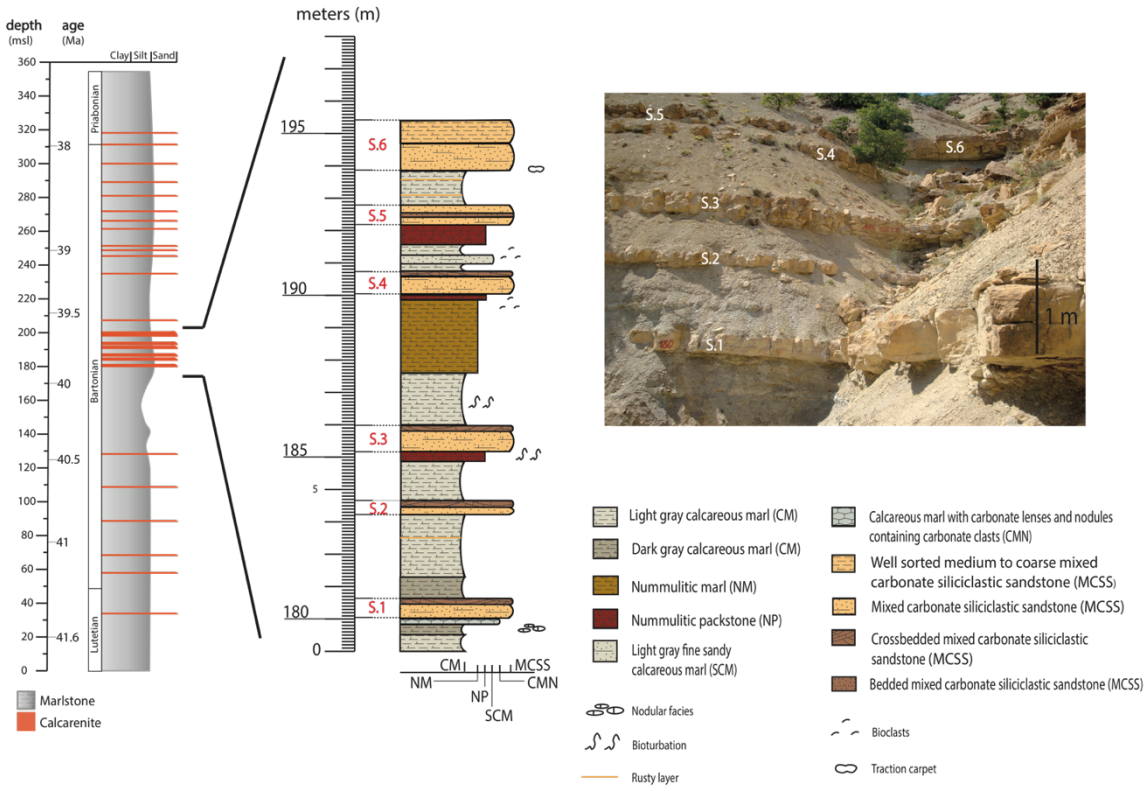

Figure 9: Detail portion of the Baskil section, from 180 to approximately 200 meters, showing changes in marlstones intercalated with calcarenite beds made from field observations. The age model was based on RODELLI et al., 2017.

Light gray to dark gray marlstone were observed in between the Sisters, including a thin layer of fine sandy calcareous marl at approximately 191 m. Sisters 1 through 4 had a similar overall texture, color and grain size. They were a mixture of carbonate and siliciclastic material with crossbedded lamination in the upper part of each bed (Figures

10A,B). Grain size were slightly coarser on the bottom and became finer towards to upper portion of each bed (Figure 10B). Bioturbation was observed in Sister 3 (Figure 10C). A nummulitic marl layer with irregular thickness ranging from 1 to approximately 2 meters was observed bellow Sister 4 (Figures 10D, E). Small layers of nummulitic packstone were also observed bellow Sisters 3, 4 and 5 (Figures 10F, G). Sisters 5 had a crossbedded lamination in the middle portion of the bed, while Sister 6 had a more homogeneous grain size throughout the entire bed with a well-defined base (Figure 10H).

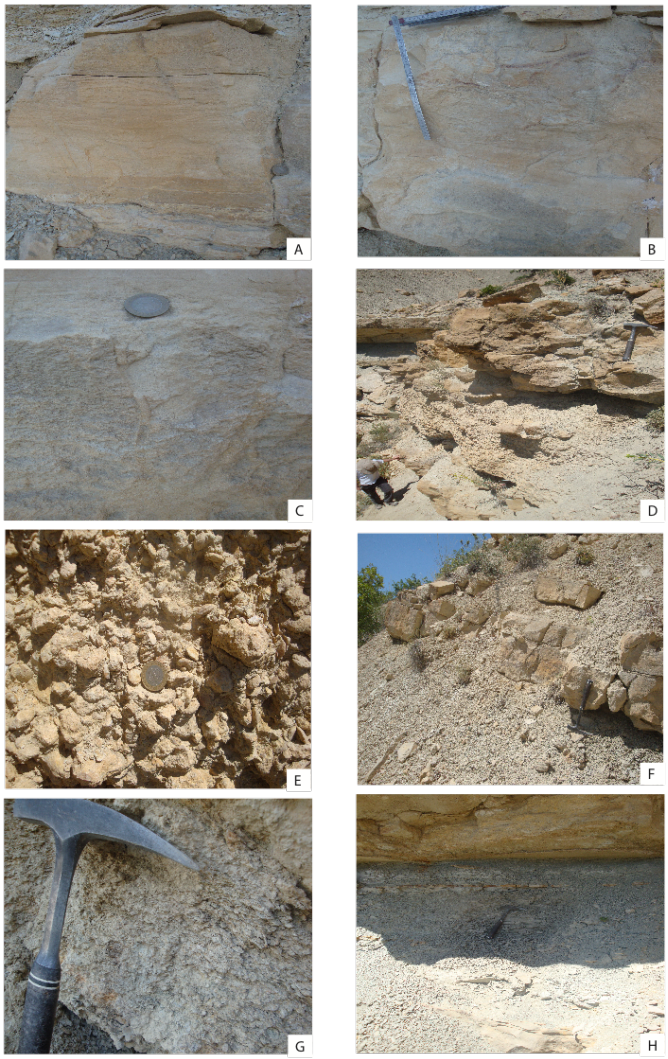

Figure 10: Detail of the Baskil section spanning the interval from 180 to 200 meters, showing (A) Sister 1with crossbedded lamination, (B) Sister 2 with slightly coarser grain size in the on the bottom and finer grains at the top, (C) bioturbation sings (vertica lines) at the top of Sister 3, (D) thick nummulitic marlstone between Sisters 3 and 4, (E) detail of nummulitic marlstone, (F) nummulitic packstone bellow Sister 5, (G) detail of nummulitic packstone, (H) well-defined base of Sister 6 with rusty layer bellow in the marlstone.

5.2 Mineralogy of marlstones

Based on mineral relative abundances and temporal trends, it was possible to subdivide the section in three intervals (I, II, and III; Figure 11 and 12). In general, the silicate group minerals have a strong negative correlation with calcite, while dolomite occurs only as a minor component and has a different trend than calcite. Clay mineral suites show significant variations in the abundances of smectite and illite, while palygorskite appears from the middle to the uppermost interval of the section.

5.2.1 Bulk mineralogy

The bulk mineral assemblages are composed mainly of quartz, albite, K-feldspar, phyllosilicates, calcite and dolomite, with variable abundances throughout the section. The lower interval (interval I; 0 msl – 125 msl) shows generally decreasing trends for quartz (14% to 7%), albite (8% to 2%), and phyllosilicates (17% to 6%), as well as an increasing trend for calcite (60% to 78%) and decreasing trend for dolomite (10% to 4%).

The middle interval (interval II; 125 msl – 275 msl) displays a significant shift in the minerals abundances. From 145 msl to 163 msl, quartz, albite, and phyllosilicates reach their highest contents (15%, 7%, and 31%, respectively), while calcite gets its minimum (44%). K-feldspar and dolomite are present only in small amounts, from ≤4% and 1% to 4%, respectively, and show no significant changes throughout the interval. At 233 msl all silicates decrease to their minimum (quartz is approximately 6%; albite 1%, K-feldspar 0%, and phyllosilicates 8%), while calcite increases up to 85%.

For the upper section (interval III; 275 msl – 357 msl), quartz, albite, K-feldspar, and phyllosilicates exhibit values similar to those in the lowermost part of the section. However, unlike interval I, the pattern shows a tendency to increase the abundances of phyllosilicates, quartz, albite and notably dolomite, while calcite decreases. Quartz

reaches up to 12%, albite up to 6% with a fairly constant trend, K-Feldspar peaks at 325 msl with 6%, while calcite presents a decreasing trend (from 82% to 68%). Dolomite, which displays low values throughout most of the section, here increases from 323 msl to 357 msl with values up to 10%.

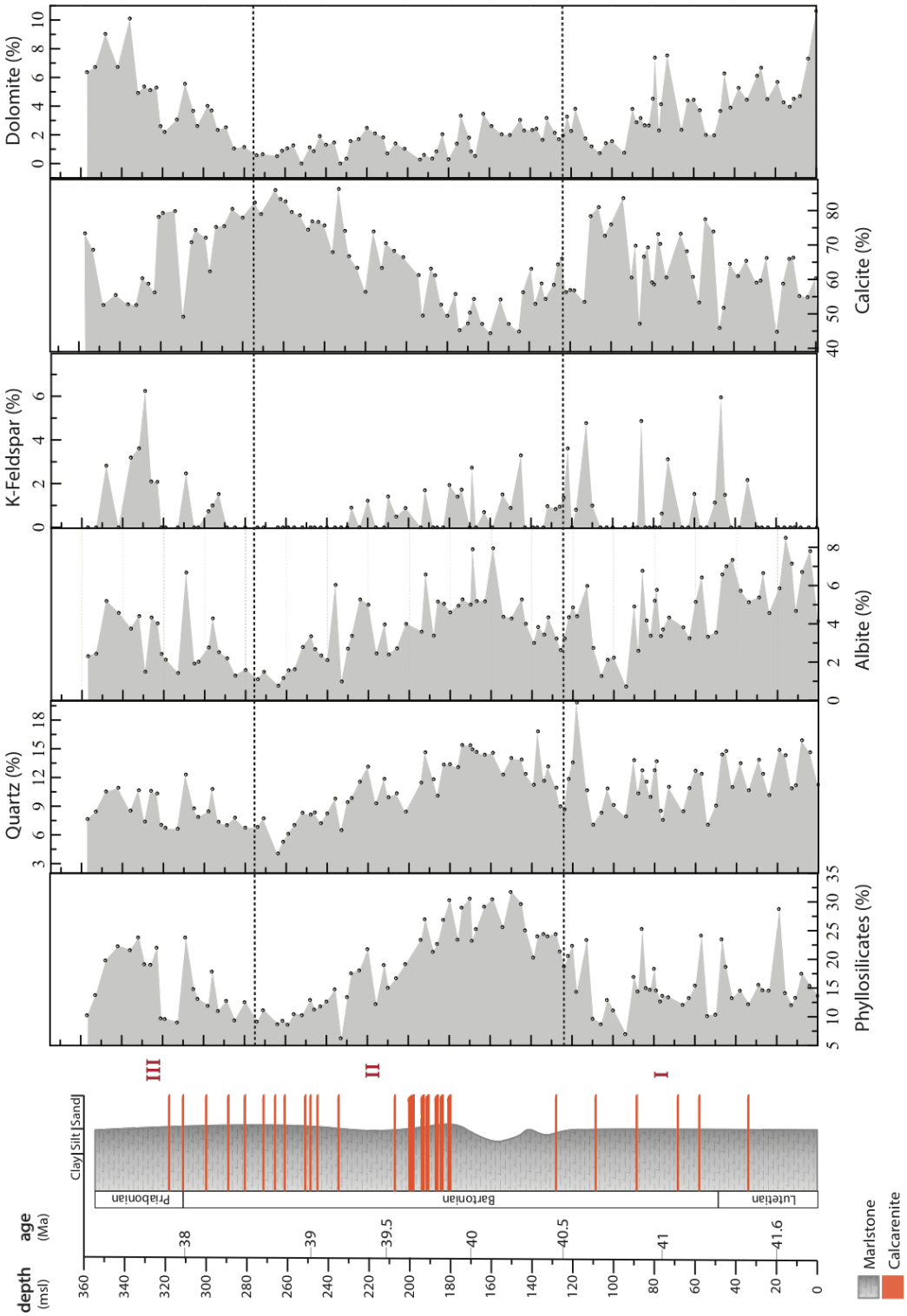

Figure 11: Bulk mineralogy of the Baskil section divided in three intervals based on temporal trends and in mineral abundances: Interval I, from 0-125 msl, interval II, from 125-275 msl, and interval III, from 275-357 msl.

5.2.2 Clay mineralogy

Clay mineral assemblages are dominated by smectite and illite (>75%), which have an inverse relationship throughout the section. In addition, palygorskite (0% to 14%), chlorite (2% to 9%), and kaolinite (1% to 3%) are less abundant. Kaolinite has a mean content of approximately 2%, which shows no significant variation within the error of the technique (FRANKE; EHRMANN, 2010).

A set of XRD patterns (Figure 13) characterizes the clay minerals variations throughout the entire section, pointing out mineralogical changes (e.g., appearance of palygorskite at 10.5 Å) in relation with the stratigraphic position. The lower interval shows smectite and illite fluctuating between 36% and 81%, and 14% and 43%, respectively. Palygorskite is mostly absent from this interval, with an exception at 47 msl (4%), while chlorite decreases slightly from about 7% to 4%. In interval II, smectite reaches a maximum content of 85%, while illite reaches a minimum of 6%. In this interval, palygorskite is found up to ~5%, while chlorite continues a decreasing trend until 159 msl (2%) and then goes back to approximately 5%. Interval III is characterized by a smectite content of about 80% until 285 msl, followed by a decreasing trend to 46% at 332 msl. In this interval, illite increases up to 34% and palygorskite reaches a maximum of about 15% at 319 msl, while chlorite shows no significant change.

Illite crystallinity shows fluctuations from approximately 0.2 to 0.6 $\Delta 2°\theta$ for the entire section. Good crystallinity (lower values, less altered) is observed in interval I with values close to 0.2 $\Delta 2°\theta$ (Figure 12). Values begin to increase at ~130 msl (interval II) with values of 0.32 and 0.44 $\Delta 2°\theta$. The uppermost interval (interval III) shows poor crystallinity (higher values, more altered) with values higher than 0.5 $\Delta 2°\theta$ above 325 msl. The illite chemistry, based on the 5/10 Å peak area ratio, has a mean value of 0.65 cps.

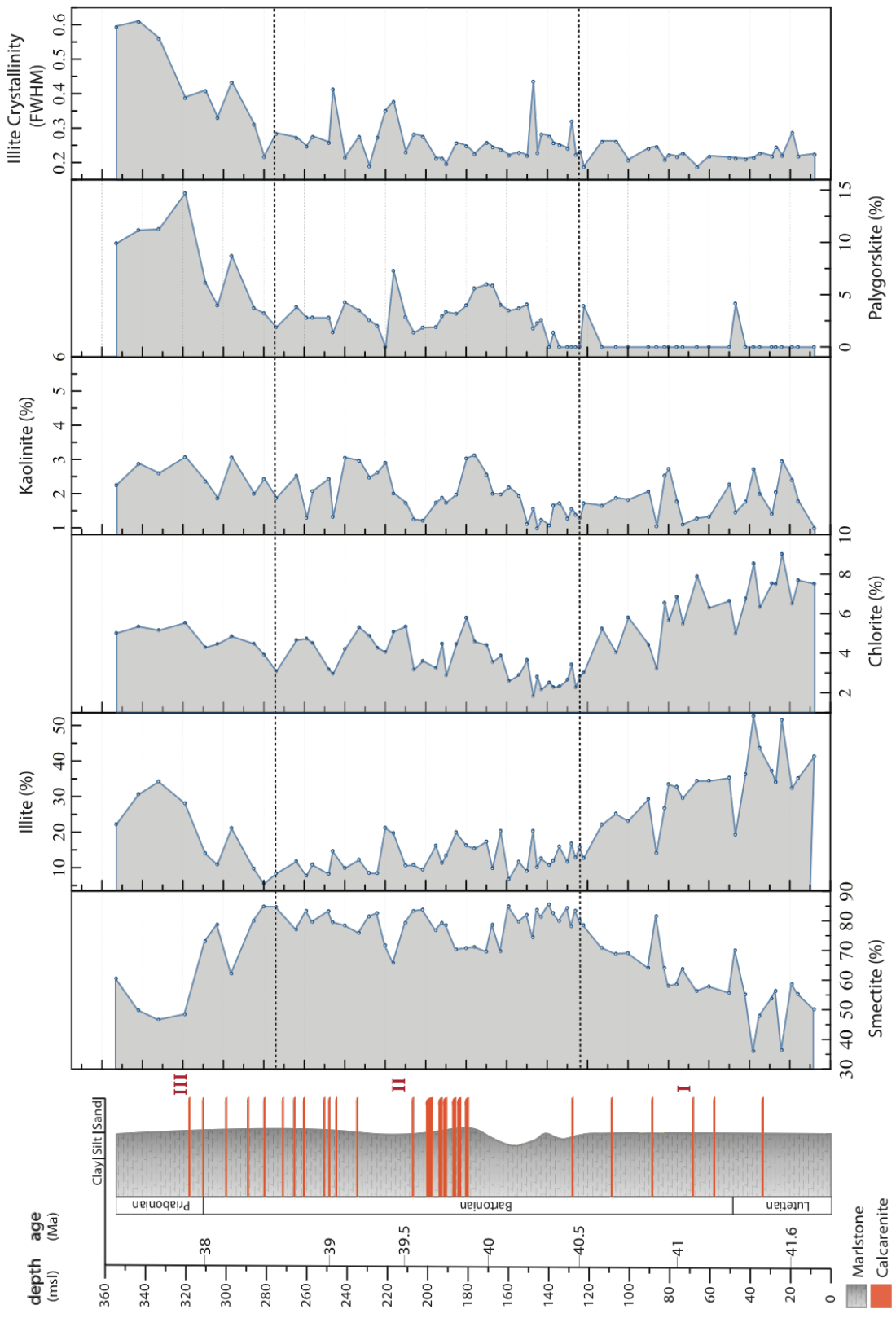

Figure 12: Clay mineralogy from the Baskil section following the same subdivisions previously used: interval I, from 0-125 msl, interval II, from 125-275 msl, and interval III, from 275-357 msl.

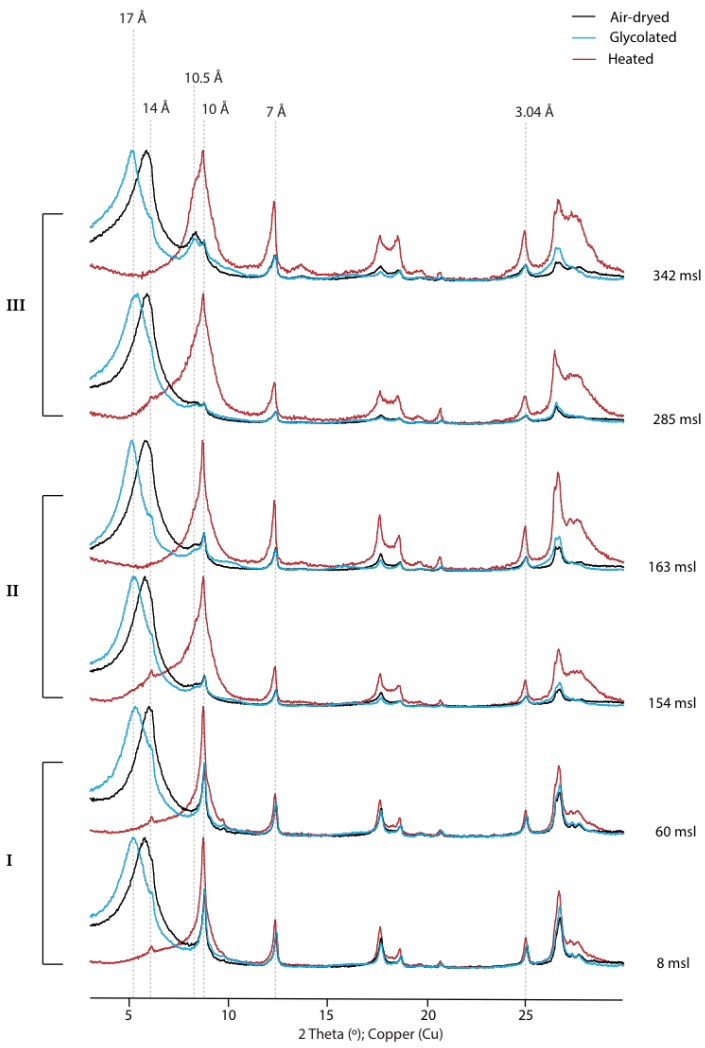

***Figure 13**:* A set of representative XRD patterns of the studied section subdivided into the three main intervals. Changes in illite crystallinity and the appearance of palygorskite are evident when comparing interval I to interval III.

Thus, the illites are more Al-rich and Mg- and Fe-poor, proximal to the composition of the muscovite. Only in the last few meters of the section, from 332 msl to 353 msl, values decrease to about 0.2, possibly showing a more biotite rich composition (Figure 23, Sup. Material).

Clay mineral ratios were applied to highlight potential environmental changes (LIMMER et al., 2012; PAYROS et al., 2015). These ratios include smectite/chlorite and (smectite+kaolinite)/(illite+chlorite), as (ChW/PhW), in a logarithmic scale to show changes from chemical to physical weathering (Figure 14). There is a significant change at approximately 125 msl, which is the beginning of interval II, where the

smectite/chlorite ratio increases significantly (~40%) when compared to the lower interval. The (ChW)/(PhW) decreases from 0% to -1%, at the same interval. However, towards the top of the section smectite/chlorite ratio follows a decreasing trend, while the ChW/ PhW remains steady until 275 msl, and then increases back to ~0%. Another typical clay parameter was the palygorskite/illite ratio (KOLLA et al., 1976; FAGEL et al., 1992) used to highlight palygorskite abundancy through the studied interval.

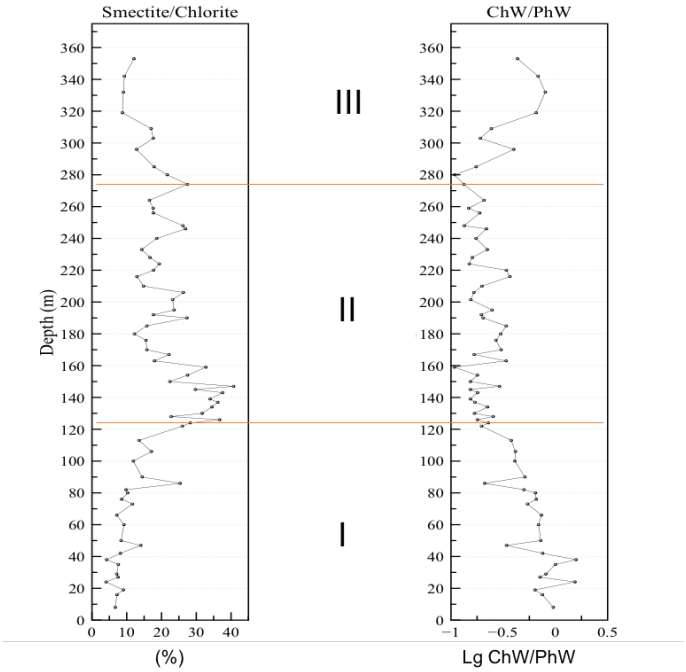

***Figure 14**:*Clay mineral ratios used as proxies to identify chemical against physical weathering. Chemical weathering (ChW) is rpresented by (smectite+kaolinite) and physical weathering (PhW) as (illite+chlorite). Chw/PhW was plotted in log scale (PAYROS et al., 2015)

5.3 SEM

Under SEM, the marlstones showed to be generally well lithified. Clay minerals occur mainly as an abundant matrix in which detrital grains of quartz or feldspar are immersed. (Figure 15A). A high abundance of smectite was observed showing an angular outline with a sometimes broken and deformed platy morphology, indicating detrital origin (Fig. 15B, C). No signs of authigenic platy clay minerals were found. Fibrous clays were also observed in interval III (Figure 15E, F). EDS analyses showed the presence of Si, Al, Mg and Fe, and traces of Ca and K, in agreement with the chemical composition

of palygorskite (EDS). Dolomite appeared in the uppermost part of the section with a rhombohedral shape (Figure 15F) followed by EDS analysis (Figure 16).

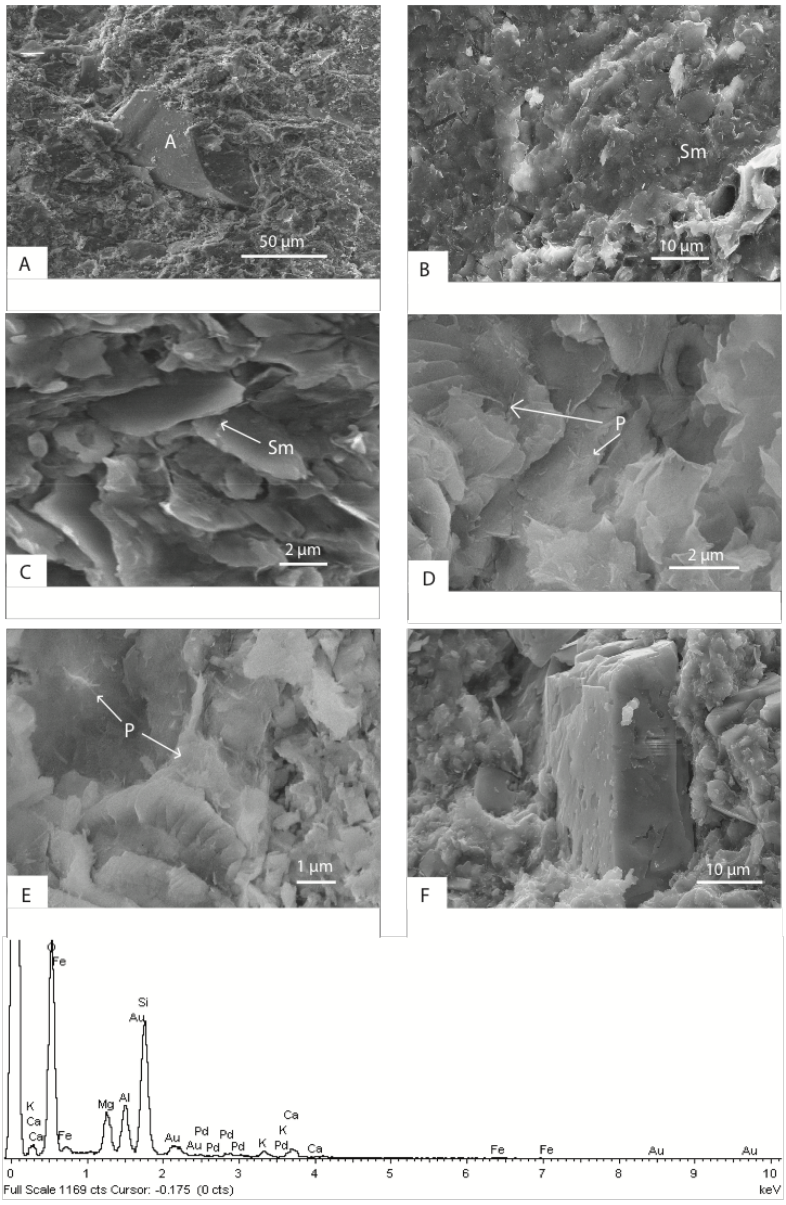

Figure 15*:* SEM images showing: (A) detrital grain of albite (A) surrounded by clay minerals at a depth of 8 msl; (B) and (C) detrital smectite (Sm) with platy morphology and "corn-flake" structure at 154 msl; (D) and (E) interwoven short clay fibers (~1 µm) of palygorskite (P); (F) Dolomite with a rhombohedral shape from interval III; EDS showing the chemical composition of the fibrous clay minerals.

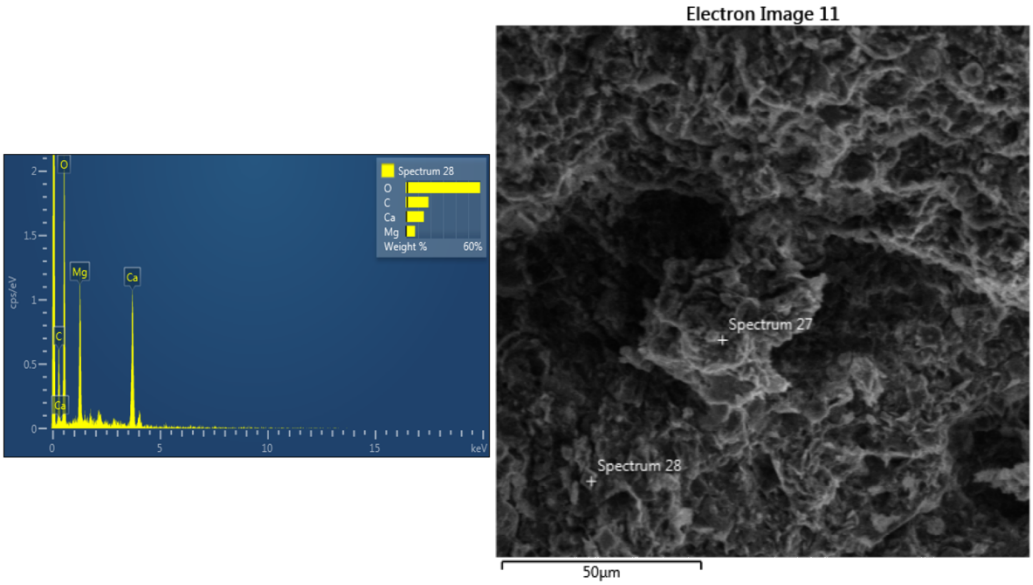

Figure 16: Spectrum 28 showing a rhombohedral dolomite

6. Interpretation and discussion

6.1 Lithostratigraphy

Calcarenite beds in the Baskil section are most likely related to mass movement events, in which an instability elsewhere at shallower depths allowed this material to be deposited at a slope environment. By looking at the field observations and considering the geology from the area, such instability was probably generated either through sea-level variations and/or due to an active tectonic regime.

Previous studies have related mass movement events, including turbidite sedimentation in slope basin, with sea-level changes, climate and tectonics (e.g. PRINS; POSTMA, 2000). Even though there is no sea-level curve for the Baskil section, sedimentation rates were decreasing (Figure 17) towards the uppermost part of the section (from 180 to 300 meters) as calcarenites were being deposited more frequently. This could indicate that after 180 meters (~ 40 Ma) the tectonic regime became more active.

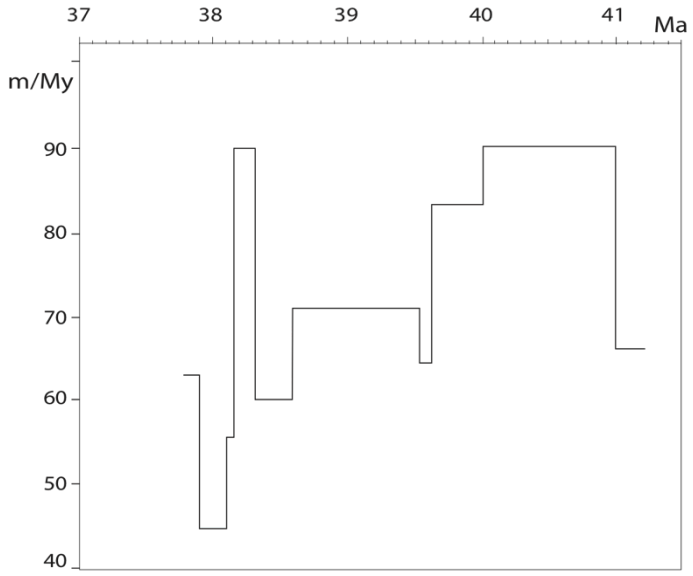

Figure 17: Sedimentation rates from the Baskil section (after RODELLI et al., 2017)

Thin-sections of the Sister beds were analyzed and they contained significant amounts of fossilized organisms (e.g. nummulites) among detrital grains (Figure 18). In addition, the presence of glauconite was observed throughout these strata (figure 18B, C, F). The formation of glauconite usually takes place in shallow-marine shelf locations with low sedimentation rates (BALDERMANN et al., 2013). The presence of the green mineral shows that the carbonates and siliciclastic material composing the Sisters was coming from a shallower platform, in which sedimentation rates were low. Moreover, other studies have related the process of glauconitization during periods of sea-level transgressions (LI et al., 2012). More work is still required in all calcarenite beds throughout the studied section, including detailed work of facies description and thin-sections, in order to obtain a conclusive result regarding the origin and forcing mechanisms related to the calcarenite deposition.

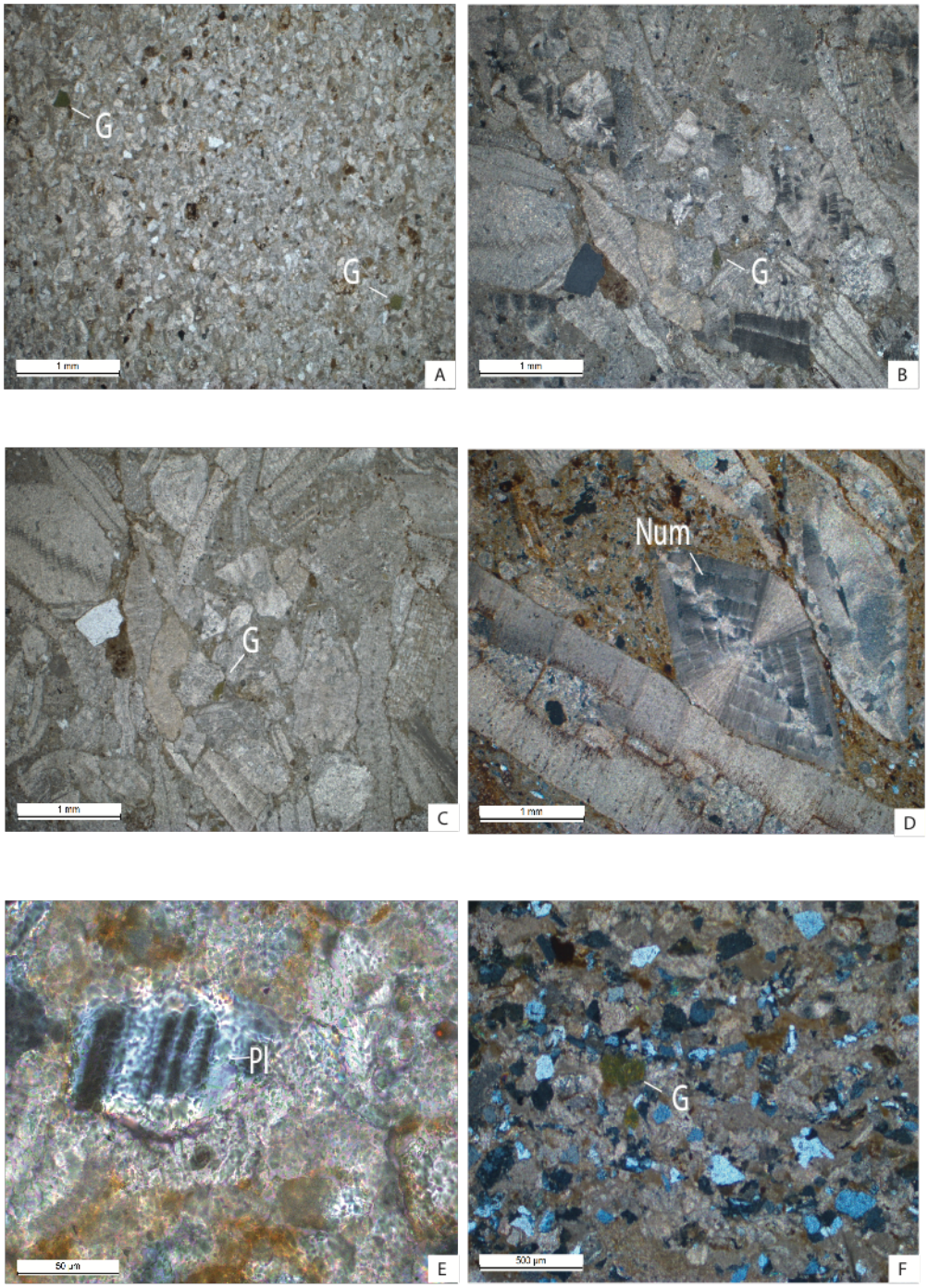

Figure 18: Glauconite grains (A,B and C) among detrital grains and fossils in Sisters 2, 3 and 4, respectively. (D) Benthic foraminifera (nummulite) in Sister 4, (E) plagioclase grain in Sister 5, and (F) closer image of glauconite grain in Sister 6.

6.2 Origin of clay- and non-clay minerals in the Baskil section

The Baskil section is characterized by two main lithologies: monotonous hemipelagic marlstones and calcarenite beds. Mineralogical variations do not reflect different rock types, since the lithological parameter is fixed and only marlstones were

analyzed. Therefore, the main processes controlling the mineralogical input and clay mineral assemblages are the composition of the source area, types of weathering of the source rocks (climate related), and offshore current patterns (FRANKE; EHRMANN, 2010).

Due to the fact that clay minerals in sedimentary rocks can be either detrital or authigenic, it is thus crucial to determine their origin before using them as proxies for environmental and/or geochemical conditions in which they formed (THIRY, 2000). Detrital clay minerals refer to inherited minerals, either from rocks (parent material) or soils developed on parent material by weathering (HILLIER, 1995). On the other hand, authigenic minerals form (a) by in situ precipitation from solution, or (b) by diagenetic alteration, or (c) by replacement of pre-existing phases within the sediment column in the depositional basin.

In the context of the Baskill section, palygorskite is considered to have an authigenic origin, which will be further discussed. The occurrence of other authigenic minerals was discarded mainly due to observations through SEM, which indicated detrital characteristics and no signs of diagenesis. Additionally, sedimentary deposit thickness did not exceed 2 km, which could also induce a diagenetic imprint (CHAMLEY, 1989; BOLLE, M.; ADATTE, 2001; CHEN et al., 2016). Despite the active tectonics in the region, the Baskil succession is tectonically undisturbed, with very little post-depositional alteration (RODELLI et al., 2017). Therefore, except for palygorskite, the clay mineral variations in this section can be interpreted as from the weathering of continental rocks and soils that were later transported into the marine depositional basin. As the entire section represents approximately 4 Myr of deposition (RODELLI et al., 2017), soils would have been able to develop and reflect the weathering and climatic changing

conditions on the continent as they altered through that period of time (THIRY; DUPUIS, 2000).

Smectite and illite are the most abundant clay minerals in the studied section and show a coeval and inverse relationship because of their different mechanisms of formation and environmental conditions under which they form. Smectite usually forms as weathering product in poorly drained soils with slow moving water, high pH, high silica activity, and abundance of cations (GALÁN, 2006). These soils form under warm and humid conditions with highly seasonality with contrasting dry and wet phases (CHAMLEY, 1989; ROBERT; CHAMLEY, 1991). The Late Cretaceous magmatic complex could be a potential source for smectite as it is commonly derived from the alteration of volcanic rocks. On the other hand, illite and chlorite are commonly products of physical erosion of low-grade metamorphic rocks, such as the Permo-Triassic metamorphic rocks, with little chemical weathering (ALIZAI et al., 2012). Kaolinite is not abundant in the section, which is expected since conditions for its formation are quite different than for the other clay minerals: very humid and warm, pervasively weathered and leached soil profiles.

The trend of the phyllosilicate's group parallels those of quartz throughout the studied succession, suggesting a common detrital origin. Conversely, calcite derives mainly from biogenic micrite, and thus has an inverse relationship with the silicate minerals. This relationship can be explained by reciprocal dilution between the terrigenous and the carbonate fractions. K-feldspar is present only in small concentrations with a mean value of 0.763 %, which is not significant for our discussion. The evolving trends of clay- and non-clay minerals are discussed below, highlighting potential source areas and environmental factors influencing assemblage variations.

Interval I, 0 – 125 msl, Lutetian – Bartonian

This interval is characterized by higher contents of illite and chlorite, and lower sedimentation rates (RODELLI et al., 2017). In the lowest part (0 – 45 msl) well-crystalized illite (mica) increases from 30% to 50% and chlorite from 7% to 9% (Figure 12). This indicates the Permo-Triassic metamorphic complex as the potential source area with a predominantly mechanical weathering regime. Quartz and albite show a decreasing trend, while calcite slightly increases. Dolomite appears more significantly in the lowest part of the section without the presence of palygorskite, indicating a possible detrital origin for the Mg-carbonate. The concentration of both illite and chlorite decrease towards the end of this interval, while smectite increases. This may reflect changes in the source area from a metamorphic to a volcanic source, in combination with a transitional change from physical to chemical weathering.

Interval II, 125 – 275 msl, Bartonian

The middle portion of the section is characterized by clay mineral assemblages dominated by smectite (83%), over illite (10%) and chlorite (2%). This indicates a change from physical to persistent and pervasive chemical weathering conditions on the continent, where the magmatic complex was the primary source for the smectite. Warmer temperatures and humid conditions contrasting with dryer periods are likely to have occurred, which is shown by the increase in poorly crystalline illite (0.45 2θ). Higher sedimentation rates prevailed until ~170 m (RODELLI et al, 2017) and started to decrease afterwards, followed by the appearance of palygorskite (Figure 12). Other silicate minerals such as quartz (16%), albite (8%), and phyllosilicates combined (35%) increased significantly from ~145 msl to 170 msl, while calcite (43%) decreases. This indicates an intensification in terrigenous input being deposited into the sedimentary basin resulting in a dilution effect of the carbonate materials. This particular interval coincides with the lowest concentration of calcite and dolomite.

The mineralogical assemblages above 170 msl begins to shift gradually to a calcite dominated period (85% at ~ 275 msl) while detrital minerals such as quartz (4%), albite (1%) and phyllosilicates (10%) decrease significantly. This biogenic carbonate "recovery" period can be interpreted as related to dryer environmental continental conditions, which caused a gradual decrease in the amount of material coming from the surrounding land and lower sedimentation rates. This is also indicated by the relatively small variations in smectite (~70 – 80%), illite (~8 – 15%), and chlorite (~3 – 5%), and by the concomitant presence of palygorskite (~1 – 6%). Dolomite maintained a relatively low concentration throughout the interval indicating not favorable conditions for its precipitation (authigenic) or no important input from a shallower carbonate environment (detrital).

To summarize, the mineral and clay mineral assemblages of interval II indicate enhanced chemical weathering, with relatively humid conditions and increasing terrigenous input into the sedimentary basin, which culminated in the beginning of interval II (125 – 170 msl). In the upper part of this interval (170 – 275 msl), the conditions started to change gradually towards drier and with less chemical weathering.

Interval III, 275 – 357 msl, Bartonian – Priabonian

The uppermost interval of the section is marked by a decrease in smectite (84 – 49%), increase in illite (5 – 34%), and increase in palygorskite (4 – 15%), suggesting: (1) change in the source area from igneous rocks back to the metamorphic complex, (2) less intense chemical weathering, and (3) changes in the water column chemistry. This clay mineral assemblage reflects source area conditions similar to those that characterize interval I. However, the illite crystallinity index is much higher (0.6 2-theta) than in interval I (0.2 2-theta), indicating that illite was altered in the terrestrial environment during deposition of interval II, and was then transported and deposited in the depositional

basin when sources changed back from igneous to metamorphic rocks. Additionally, the combination of higher content of palygorskite (15%), the increase in dolomite (10%), and low sedimentation rates points to a Mg-richer environment, probably with warmer and more saline bottom water condition (THIRY; PLETSCH, 2011).

As mentioned above, the palygorskite found in the Baskil section is interpreted to have formed *in situ*, which most likely precipitated in the pore spaces of near-surface sediments (Figure 15D,E). Indeed, it is highly unlikely that small delicate fibers (~1 μm) were reworked from land or shallow-water environments and transported to the depositional basin at water depths of ~300 to 600 m (RODELLI et al., 2017). Authigenic palygorskite has been observed in deep-sea sediments and it has been proposed to have required changes at the seabed and in the water column, such as reduced sedimentation rates, elevated ambient temperature, and high Mg and Si concentrations (PLETSCH, 1998, 2001; THIRY; PLETSCH, 2011). These conditions are similar to the ones required for the formation of authigenic/diagenetic dolomite, which also indicate a magnesium-rich environment (CHAHI; DUPLAY; LUCAS, 1993; THIRY; JACQUIN, 1993; THIRY; PLETSCH, 2011); dolomite and palygorskite occur together in the uppermost interval (interval III) of the Baskil section, and thus the environmental conditions proposed for their formation were likely extant in the Elazig basin.

Previous work invoked the possibility of elevated deep-sea temperatures, salinity, and magnesium- and silica-rich waters to account for the formation of authigenic palygorskite during the lower Eocene (PLETSCH, 1998, 2001; SHOVAL, 2004). Since the possibility of detrital palygorskite was unlikely, the conditions in the water column must have changed. Magnesium could have been supplied by saline bottom water, perhaps fed from an evaporative platform, allowing the formation of palygorskite and dolomite (THIRY; PLETSCH, 2011). Evidence of such an evaporative environment in

central Turkey is marked by the occurrence of marine palygorskite, which appears in evaporative deposits spanning the Paleocene and Eocene within three other sedimentary basins (e.g. Sivas, Hekimhan and Darende basin) in relatively close proximity to the Elazig basin, where the Baskil section lies (PALMER; HELVACÍ; FALLICK, 2004; YALÇIN; BOZKAYA, 1995, 2011; BOOTH et al., 2014).

The combination of leaching of lightly increased amounts of silicate minerals with the increase in magnesium being fed from shallower environments, and an additional increase in temperature and salinity could have provided the necessary conditions for the formation of the fibrous clay minerals. Changes in ocean circulation, including stratification of the water column, have been noted for warmer periods on Earth from the Late Cretaceous to the Eocene (BRASS; SOUTHAM; PETERSON, 1982; MILLER, 1992; KROON et al., 2000; PAK; SHOVAL, 2004; THIRY; PLETSCH, 2011). Here we suggest that a stratified water column occurred in the Baskil section due to changes in circulation, which allowed conditions for the formation of authigenic palygorskite accompanied by dolomite in a Mg- and Si-rich environment under low sedimentation rates.

The clay mineral assemblages in interval III can be attributed to various processes. (1) There was a change in source area that provided more weathered illite, previously developed, and then (2) less intense chemical weathering on the continent. (3) Enhanced stratification of the water column may have been caused by changes in ocean circulation, in combination with dryer and more evaporative conditions on the adjacent land and shallower marine environments, and with lower sedimentation rates. These conditions would have promoted warmer and saline bottom water, rich in magnesium, favorable for palygorskite and dolomite formation in the deeper-water depositional basin. (4) A sea-level retreat occurred in the Neo-Tethys from approximately 41 Myr ago until the Eocene-

Oligocene boundary (MILLER, 2005; BOSBOOM et al., 2011; WANG et al., 2013b ; BOSBOOM; GUO, 2014). This exposed, reworked, and transported material from a shallower continental margin to a deeper basin was not enough to increase sedimentation rates but could explain the small increase in silicate minerals.

6.3 A mineralogical evidence of the MECO in the Baskil section?

Our well-dated succession can be used to correlate the mineralogical variations to global climatic changes known to have occurred during the middle Eocene. The global warming event that took place during the middle Eocene, also known as MECO, occurred at approximately 40.5 Myr ago and lasted for almost 500 ka (BOHATY; ZACHOS, 2003; BOHATY et al., 2009). Despite its clear stable isotopic signature, which was found in the Atlantic, Pacific, and Indian Oceans (BOHATY et al., 2009; EDGAR et al., 2010; PASCHER et al., 2015), as well as in the Tethys (JOVANE et al., 2007; LUCIANI et al., 2010; SPOFFORTH et al., 2010; DAWBER et al., 2011; Savian et al., 2014), the climatic mechanism responsible for this event are still not well understood. Computer model projections, when compared to observed data, fail to explain the long duration of the warming conditions, as well as their abrupt end (SLUIJS et al., 2013).

In the Baskil section, the 40.5 to ~40 Ma interval ranges from a depth of 125 msl to 163 msl and is clearly marked by increase in smectite (>80%), decrease in illite (<10%) and palygorskite starts to appear more significantly during and after the event (Figure 12, 19). Additionaly, the clear oxygen isotope ($\delta^{18}O$) excursion from benthic and planktonic foraminifera (GIORGIONI, in prep) confirms the mineralogical signature of the event (Figure 19). This shift to smectite as the dominant clay mineral not only indicates a potential change in source area characterized by volcanic material, but also a climatic change, where warmer conditions with moderate humidity would favor smectite

formation and deposition prior to the MECO peak warming. Furthermore, the appearance of authigenic palygorskite, shown with palygorskite/illite ratio, is suggested to be product of changes in the water column possibly related to changes in circulation patterns. The increase in palygorskite is concomitant with the global warming event (Figure 19). A divergence between the $\delta^{18}O$ curves of the shallow- and deep-water dwelling planktonic foraminifera after the event suggests a more stratified water column in the Neo-Tethys.

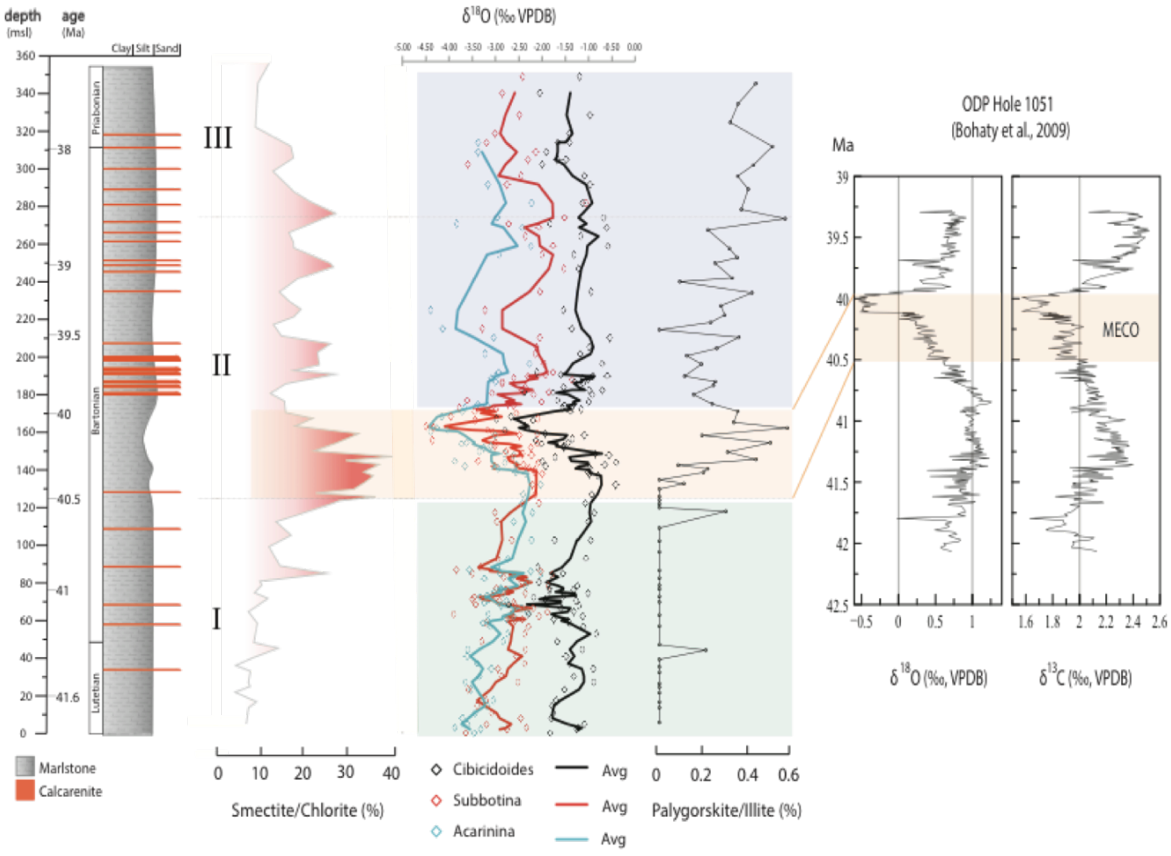

Figure 19: Clay mineral ratios and stable oxygen isotopes from planktonic and benthic foraminifera (Giorgioni, in prep.) marking the Middle Eocene Climatic Optimum (MECO) in the Baskil section.

Clay minerals have been used to identify warmer/cooler periods such as the PETM, the EECO, and the Eocene/Oligocene transition. For example, the increase in kaolinite content indicates warmer and humid conditions during the PETM at many locations, such as North and South Atlantic, Antarctica, New Zealand, China, Egypt, Israel, Tunisia, Kazakhstan, Spain, and England (ROBERT; CHAMLEY, 1991;

ROBERT; KENNET, 1994; KAIKO et al., 1996; GAWENDA et al., 1999; GIBSON; BYBELL; MASON, 2000; ERNST et al., 2006; SCHULTE; SCHEIBNER; SPEIJER, 2011; SOLIMAN et al., 2011; JOHN et al., 2012; BORNEMANN et al., 2014; PUJALTE; BACETA; SCHMITZ, 2015; CHEN et al., 2016; KEMP et al., 2016). The EECO proxies were identified in the western Pyrenees and in China, also with an increase in kaolinite, however towards the end of the period, dryer conditions may have prevailed (WANG et al., 2013a; PAYROS et al., 2015). The Eocene/Oligocene transition, characterized by cooling climate, is marked by a decrease in kaolinite and smectite and a corresponding increase in illite and chlorite (EHRMANN; MACKENSEN, 1992; DIESTER-HAAS; ROBERT; CHAMLEY, 1996; WANG et al., 2013a; ZHANG; GUO, 2014). The MECO, however, has only been mineralogically characterized at Monte Cagnero (MCA, Italy) and in the western Indian Ocean (ODP Site 711), where an increase in smectite content has been observed associated with the warming phase (SAVIAN et al., 2014, 2016). The same samples from the Indian Ocean (ODP Site 711) were analyzed with the methods used for this study. The results showed consistency, where smectite increases during the MECO, even though calcite was removed through sample preaparation and only insignificant amount of quartz was present in the less then 2 μm (Figure 20).

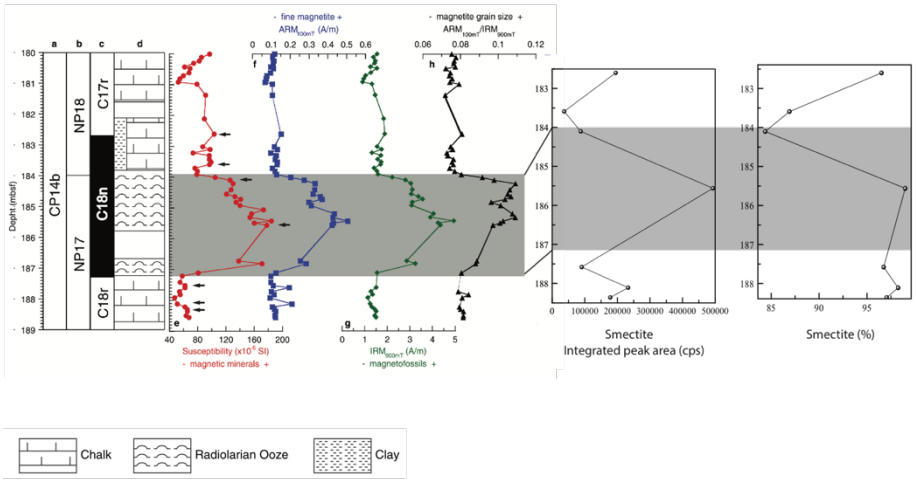

Figure 20: Increase in smectite integrated peak area and percentage during the MECO interval (after SAVIAN et al., 2016).

The increase in smectite in the Baskil section is well dated at ~40.5 Ma, based on the age model of RODELLI et al. (2017), and thus may be related to the changing climatic conditions during the MECO. Moreover, this is the first evidence of palygorskite appearance during the event. Clay mineral ratios were employed to correlate major changes during the warming periods. Chemically weathered produced smectite and kaolinite contrasts with physically eroded illite and chlorite, providing a proxy for chemical weathering, which in turns also shows warmer climate (LIMMER et al., 2012; PAYROS et al., 2015) (Figure 21).

Even though records expressing continental conditions during the MECO are still scarce, previous studies have shown warm and semi-arid to sub-humid conditions in western North America (METHNER et al., 2016) followed by aridification (BOSBOOM et al., 2014). This is consistent with our results showing an increase in smectite and decrease in illite and chlorite, which indicate warmer conditions. Moreover, this clay mineral assemblage is maintained until ~275 msl (38.5 Myr ago), with the additional increasing trend of authigenic palygorskite. This indicates that chemical weathering

conditions predominated in the Baskil region also after the MECO, accompanied by dryer periods and paleoceanographic changes. Further work is necessary to verify the relationship between the MECO and the paleoceanographic evolution of the region. However, this is the first study showing a possible change in the water column right after the MECO event in the Neo-Tethys and coincides with previous works showing dryer conditions after the event.

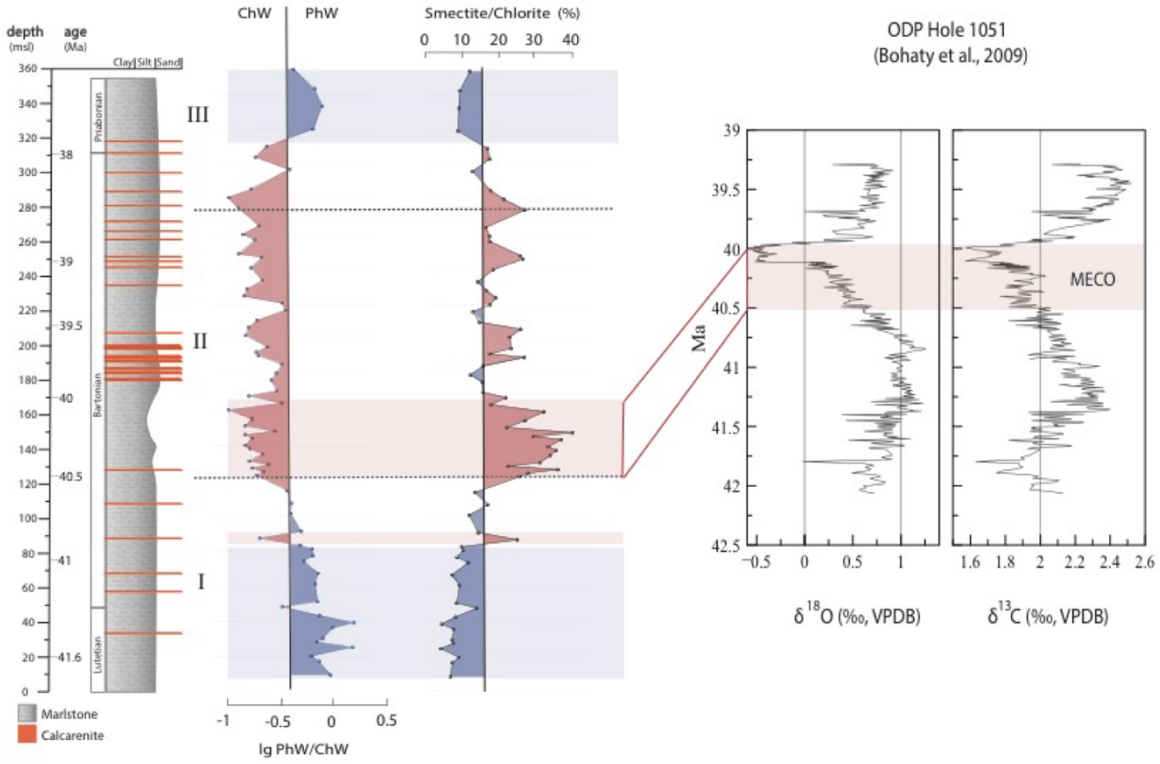

Figure 21: Clay mineral ratios showing that warmer conditions were maintained after the warming event with chemical weathering (ChW) regime on land until approximately 38.5 Ma.

7. Conclusions

This study shows that non-clay and clay minerals variations along a well-preserved sedimentary section provide reliable proxies for detrital source areas and weathering regimes. Moreover, the appearance of authigenic minerals were used as an indicator of changes in the water column conditions, which was the first occurrence registered during a global warming period. The dominant condition of abundant well-

crystallized illite in the lowermost interval of the studied section (interval I) changed gradually to a smectite dominant interval (interval II), coinciding with the onset of the Middle Eocene Climatic Optimum. This is interpreted as from a change in source area, from a metamorphic to magmatic rocks, in combination with changes from physical to chemical weathering. Additionally, increasing sedimentation rates indicate increased erosion from a warmer and more humid climate on land at the beginning of interval II. The smectite content slightly decreased after 40 Ma, but its dominance was maintained until 38.5 Ma. In addition, the uppermost interval (interval III) shows lower sedimentation rates, slight increase of silicates, accompanied by increase in weathered illite and especially palygorskite and dolomite. This indicates a change in the source area providing previously weathered illite, and changes in the water column that favored the formation of palygorskite and dolomite. The hypothesis tested was supported by the data, which showed an increase in smectite during a warmer period. The mineralogical evolution of the Baskil section reflects how source-areas and weathering regimes changed through time on land, how environmental changes occurred concomitantly on the continent and in a restricted ocean, and how these changes can be related to global (i.e. MECO) and/or local to regional processes (Figure 22).

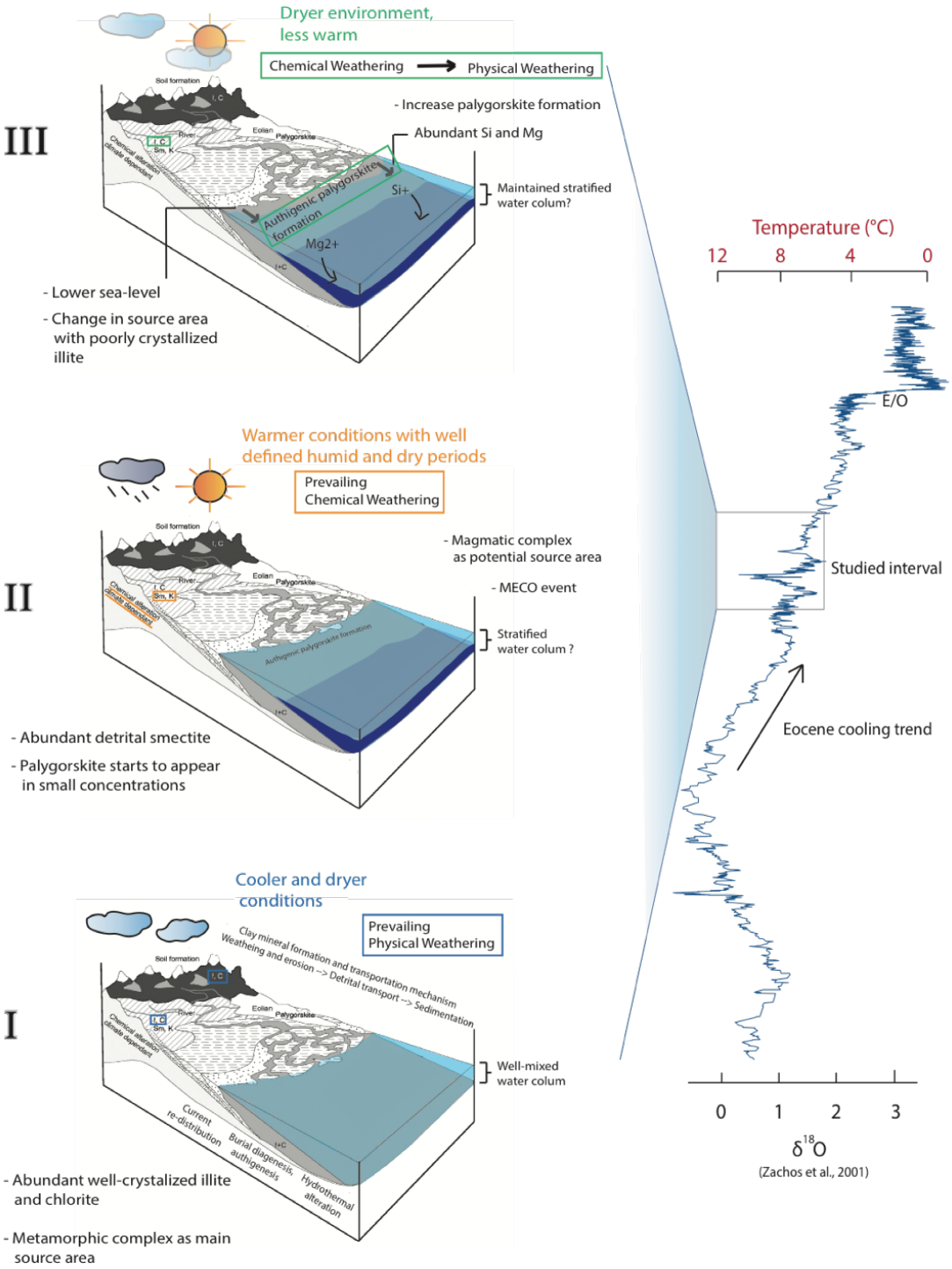

Figure 22:Mineralogical evolution in the Baskil section representing climatic conditions on land and possible changes in the water column during the studied interval (box diagram after FAGEL, 2007).

8. References

AKSOY, E.; TÜRKMEN, İ.; TURAN, M. Tectonics and sedimentation in convergent margin basins: an example from the Tertiary Elazığ basin, Eastern Turkey. *Journal of Asian Earth Sciences*, v. 25, n. 3, p. 459–472, jun. 2005.

ALIZAI, A. et al. Clay mineral variations in Holocene terrestrial sediments from the Indus Basin. *Quaternary Research*, v. 77, n. 3, p. 368–381, maio 2012.

BALDERMANN, A. et al. The rate and mechanism of deep-sea glauconite formation at the Ivory Coast-Ghana Marginal Ridge. *Clays and Clay Minerals*, v. 61, n. 3, p. 258–276, 2013.

BINGÖL, A. F.; BEYARSLAN, M. The geochemistry and petrology of Elazığ magmatics. *Proceedings of 30th Anniversary Symposium of Geology Department, Karadeniz Technical University, Trabzon–Turkey*, p. 208–224, 1996.

BISCAYE. Mineralogy and Sedimentation of Recent Deep-Sea Clay in the Atlantic Ocean and Adjacent Seas and Oceans. *Geological Society of America Bulletin*, 1965.

BLAKE, D. et al. Characterization and calibration of the CheMin mineralogical instrument on Mars Science Laboratory. *Space Science Reviews*, v. 170, n. 1–4, p. 341–399, 2012.

BOHATY, S. M. et al. Coupled greenhouse warming and deep-sea acidification in the middle Eocene. *Paleoceanography*, v. 24, n. 2, p. n/a-n/a, jun. 2009.

BOHATY, S. M.; ZACHOS, J. C. Significant Southern Ocean warming event in the late middle Eocene. *Geology*, v. 31, n. 11, p. 1017–1020, 2003.

BOLLE, M., P.; ADATTE, T. Palaeocene-early Eocene climatic evolution in the Tethyan realm : clay mineral evidence. *Clay Minerals*, n. 36, p. 249–261, 2001.

BOOTH, M. G. et al. Late Cretaceous to Late Eocene Hekimhan Basin (Central Eastern Turkey) as a supra-ophiolite sedimentary/magmatic basin related to the later stages of closure of Neotethys. *Tectonophysics*, v. 635, p. 6–32, 2014.

BORCHERS, A. et al. Mineralogy of glaciomarine sediments from the Prydz Bay–Kerguelen region: relation to modern depositional environments. *Antarctic Science*, v. 23, n. 2, p. 164–179, 16 abr. 2011.

BORNEMANN, A. et al. Persistent environmental change after the Paleocene–Eocene Thermal Maximum in the eastern North Atlantic. *Earth and Planetary Science Letters*, v. 394, p. 70–81, maio 2014.

BOSBOOM, R. E. et al. Late Eocene sea retreat from the Tarim Basin (west China) and concomitant Asian paleoenvironmental change. *Palaeogeography, Palaeoclimatology,*

Palaeoecology, v. 299, n. 3–4, p. 385–398, 2011.

BOSBOOM, R. E. et al. Aridification in continental Asia after the Middle Eocene Climatic Optimum (MECO). *Earth and Planetary Science Letters*, v. 389, p. 34–42, mar. 2014.

BOSBOOM, R. E.; GUO, Z. Aridification in continental Asia after the Middle Eocene Climatic Optimum (MECO). *Earth and Planetary Science Letters*, v. 389, n. March, p. 34–42, 2014.

BRASS, G.; SOUTHAM, J.; PETERSON, W. H. Warm saline bottom water in the ancient ocean. *Nature*, v. 296, p. 620–623, 1982.

ÇELIK, H. The effects of linear coarse-grained slope channel bodies on the orientations of fold developments: A case study from the Middle Eocene-Lower Oligocene Ki{dotless}rkgeçit Formation, Elazi{dotless}ğ, eastern Turkey. *Turkish Journal of Earth Sciences*, v. 22, n. 2, p. 320–338, 2013.

CHAHI, A.; DUPLAY, J.; LUCAS, J. Analyses of palygorskites and associated clays from the origin of formation chatky dotomite pink mart pink gypsite. *Clays and Clay Minerals***,** v. 41, n. 4, p. 401–411, 1993.

CHAMLEY, H. *Clay sedimentology*. Berlin: Springer, 1989.

CHEN, Q.; LIU, Z.; KISSEL, C. Clay mineralogical and geochemical proxies of the East Asian summer monsoon evolution in the South China Sea during Late Quaternary. *Scientific Reports*, v. 7, p. 42083, 2017.

CHEN, Z. et al. Increased precipitation and weathering across the Paleocene-Eocene Thermal Maximum in central China. *Geochemistry, Geophysics, Geosystems*, v. 17, n. 6, p. 2286–2297, jun. 2016.

COCCIONI, R. et al. An integrated stratigraphic record of the Palaeocene-lower Eocene at Gubbio (Italy): new insights into the early Palaeogene hyperthermals and carbon isotope excursions. *Terra Nova*, v. 24, n. 5, p. 380–386, out. 2012.

CRONIN, B. T. et al. Equilibrium profile development in graded deep-water slopes: Eocene, Eastern Turkey. *Journal of the Geological Society*, v. 157, n. 5, p. 943–955, 2000.

CRONIN, B. T. et al. Deep- water slope channel complex fill and overbank architecture of the Tinker Channel, Kirkgecit Formation, Turkey. In: *Atlas of deep-water turbidite systems*. [s.l: s.n.]. p. 363–367, 2007.

DAWBER, C. F. et al. Glacioeustasy during the middle Eocene? Insights from the stratigraphy of the Hampshire Basin, UK. *Palaeogeography, Palaeoclimatology, Palaeoecology*, v. 300, n. 1–4, p. 84–100, fev. 2011.

DIESTER-HAAS, L.; ROBERT, C.; CHAMLEY, H. The Eocene-Oligocene preglacial-glacial

transition in the Atlantic sector of the Southern Ocean (ODP Site 690). *Marine Geology*, v. 131, p. 123–149, 1996.

DONOVAN, S. K.; PICKERILL, R. K. On marls and marlstones. v. 39, n. 39, p. 127–128, 2013.

EBERL, D. Clay mineral formation and transformation in rocks and soils. *Phil. Trans. R. Soc. Lond. A*, v. 311, p. 241–257, 1984.

EDGAR, K. M. et al. New biostratigraphic , magnetostratigraphic and isotopic insights into the Middle Eocene Climatic Optimum in low latitudes. *Palaeogeography, Palaeoclimatology, Palaeoecology*, v. 297, n. 3–4, p. 670–682, 2010.

EHLMANN, B. L. et al. Subsurface water and clay mineral formation during the early history of Mars. *Nature*, v. 479, n. 7371, p. 53–60, 2011.

EHRMANN, W. et al. A distal 145 ka sediment record of Nile discharge and East African monsoon variability. *Climate of the Past Discussions*, v. 11, n. 5, p. 4273–4308, 7 set. 2015.

EHRMANN, W.; SETTI, M.; MARINONI, L. Clay minerals in Cenozoic sediments off Cape Roberts (McMurdo Sound, Antarctica) reveal palaeoclimatic history. *Palaeogeography, Palaeoclimatology, Palaeoecology*, v. 229, n. 3, p. 187–211, dez. 2005.

EHRMANN, W. U.; MACKENSEN, A. Sedimentological evidence for the formation of an East Antarctic ice sheet in Eocene / Oligocene time. *Palaeogeography, Palaeoclimatology, Palaeoecology*, v. 93, p. 85–112, 1992.

ERNST, S. R. et al. Environmental perturbation in the southern Tethys across the Paleocene/Eocene boundary (Dababiya, Egypt): Foraminiferal and clay mineral records. *Marine Micropaleontology*, v. 60, n. 1, p. 89–111, jun. 2006.

ESQUEVIN, J. Influence de la composition chimique des illites sur le cristallinite. *Bull. Cent. Rech. Pau S.N.P.A,* v. 3, p. 147–154, 1969.

FAGEL, N. et al. des minéraux sédimentaires argileux pour la reconstitution des variations paléoclimatiques à court terme en Mer d ' Arabie. *Oceanologica Acta*, v. 15, p. 125–136, 1992.

FAGEL, N. Clay Minerals, Deep Circulation and Climate. In: *Paleoceanography of the Late Cenozoic*. [s.l.] Elsevier B.V., 2007. v. 1p. 139–184.

FAGEL, N.; ROBERT, C.; HILLAIRE-MARCEL, C. Clay mineral signature of the NW Atlantic Boundary Undercurrent. *Marine Geology*, v. 130, n. 1–2, p. 19–28, 1996.

FOSTER, G. L. et al. Future climate forcing potentially without precedent in the last 420 million years. *Nature Communications*, v. 8, p. 14845, 2017.

FRANKE, D.; EHRMANN, W. Neogene clay mineral assemblages in the AND-2A drill core (McMurdo Sound, Antarctica) and their implications for environmental change. *Palaeogeography, Palaeoclimatology, Palaeoecology*, v. 286, n. 1–2, p. 55–65, fev. 2010.

GALÁN, E. Genesis of Clay Minerals. In: *Developments in Clay Science*. [s.l: s.n.]. v. 1p. 1129–1162, 2006.

GALÁN, E.; POZO, M. Palygorskite and sepiolite deposits in continental environments. Description, genetic patterns and sedimentary settings. In: *Developments in Clay Science* [s.l: s.n.]. v. 3, p. 125-173, 2011.

GALEOTTI, S. et al. Orbital chronology of Early Eocene hyperthermals from the Contessa Road section, central Italy. *Earth and Planetary Science Letters*, v. 290, n. 1–2, p. 192–200, 2010.

GAWENDA, P. et al. Climate and bioproductivity control on carbonate turbidite sedimentation (Paleocene to earliest Eocene, Gulf of Biscay, Zumaia, Spain). *Journal of Sedimentary Research*, v. 69, p. 1253–1261, 1999.

GIBSON, T. G.; BYBELL, L. M.; MASON, D. B. Stratigraphic and climatic implications of clay mineral changes around the Paleocene/Eocene boundary of the northeastern US margin. *Sedimentary Geology*, v. 134, n. 1–2, p. 65–92, jul. 2000.

GRIFFIN, J. J.; WINDOM, H.; GOLDBERG, E. D. The distribution of clay minerals in the World Ocean. *Deep-Sea Research*, v. 15, p. 433–459, 1968.

GUO, J.; UNDERWOOD, M. B. Data report: refined method for calculating percentages of kaolinite and chlorite from X-ray diffraction data, with application to the Nankai margin of southwest Japan. In: *Proceedings of the Integrated Ocean Drilling Program*. [s.l: s.n.]. v. 314, 2011.

HEIN, J. R. et al. Clay-mineral suites, sources, and inferred dispersal routes: Southern California continental shelf. *Marine Environmental Research*, v. 56, n. 1–2, p. 79–102, jul. 2003.

HEIN, J. R.; SCHOLL, D. W.; GUTMACHER, C. E. Neogene clay minerals of the Far NW Pacific and southern Bering Sea : Sedimentation and Diagenesis. *Proceedings of the International Clay Conference*, 1976.

HILLIER, S. Erosion, sedimentation and sedimentary origin of clays. In: *Origin and Mineralogy of Clays: Clays and the Environment*. [s.l: s.n.]. p. 162–219.

HILLIER, S. Quantitative analysis of clay and other minerals in sandstones by X-ray powder diffraction (XRPD). In: WORDEN, R. H.; MORAD (Eds.). . *Clay Mineral Cements in*

Sandstones. [s.l.] International Association of Sedimentologists, 2003. v. 34p. 213–251.

JOHN, C. M. et al. Clay assemblage and oxygen isotopic constraints on the weathering response to the Paleocene-Eocene thermal maximum, east coast of North America. *Geology*, v. 40, n. 7, p. 591–594, 1 jul. 2012.

JOVANE, L. et al. The middle Eocene climatic optimum event in the Contessa Highway section, Umbrian Apennines, Italy. *Geological Society of America Bulletin*, v. 119, n. 3–4, p. 413–427, 1 mar. 2007.

KAIKO, K. et al. Latest Paleocene benthic foraminiferal extinction and environmental changes at Tawanui, New Zealand. *Paleoceanography*, v. 11, n. 4, p. 447–465, 1996.

KELLER, W. D.; REYNOLDS, R. C.; INOUE, A. MORPHOLOGY OF CLAY MINERALS IN THE SMECTITE-TO-ILLITE CONVERSION SERIES BY SCANNING ELECTRON MICROSCOPY. *Clays and Clay Minerals*, v. 34, n. 2, p. 187–197, 1986.

KEMP, S. J. et al. Palaeoclimatic implications of high- resolution clay mineral assemblages preceding and across the onset of the Palaeocene – Eocene Thermal Maximum , North Sea Basin. *Clay Minerals*, v. 51, p. 793–813, 2016.

KOLLA, V.; HENDERSON, L.; BISCAYE, P. E. Clay mineralogy and sedimentation in the western Indian ocean. *Deep Sea Research and Oceanographic Abstracts*, v. 23, n. 10, p. 949–961, 1973.

KROON, D. et al. Exerpts from the Final Report of the JOIDES Extreme Climates Program. *Joides Journal*, v. 26, n. 1, p. 17–25, 2000.

LAMY, F.; HEBBELN, D.; WEFER, G. Late quaternary precessional cycles of terrigenous sediment input off the Norte Chico, Chile (27.5°S) and palaeoclimatic implications. *Palaeogeography, Palaeoclimatology, Palaeoecology*, v. 141, n. 3–4, p. 233–251, 1998.

LI, X. et al. Mineralogical characteristics and geological significance of Albian (Early Cretaceous) glauconite in Zanda, southwestern Tibet, China. *Clay Minerals*, v. 47, n. 1, p. 45–58, 2012.

LIMMER, D. R. et al. Chemical weathering and provenance evolution of Holocene–Recent sediments from the Western Indus Shelf, Northern Arabian Sea inferred from physical and mineralogical properties. *Marine Geology*, v. 326–328, n. August, p. 101–115, out. 2012.

LIU, Z. et al. Clay mineral assemblages in the northern South China Sea: Implications for East Asian monsoon evolution over the past 2 million years. *Marine Geology*, v. 201, n. 1–3, p. 133–146, 2003.

LOURENS, L. et al. Astronomical pacing of late Palaeocene to early Eocene global warming

events. *Nature*, v. 435, n. 7045, p. 1083–1087, 2005.

LUCIANI, V. et al. Ecological and evolutionary response of Tethyan planktonic foraminifera to the middle Eocene climatic optimum (MECO) from the Alano section (NE Italy). *Palaeogeography, Palaeoclimatology, Palaeoecology*, v. 292, n. 1–2, p. 82–95, jun. 2010.

MCREYNOLDS, T. E.; SKAGGS, S. A.; SCHROEDER, P. A. Feldspar and Clay Mineralogy. *Woodland pottery sourcing in the Carolina Sandhills*, n. 29, 2008.

MERRIMAN, R. J. Clay minerals and sedimentary basin history. *European Journal of Mineralogy*, v. 17, n. 1, p. 7–20, 2005.

METHNER, K. et al. Rapid Middle Eocene temperature change in western North America. *Earth and Planetary Science Letters*, v. 450, n. September, p. 132–139, set. 2016.

MILLER, K. G. The Phanerozoic Record of Global Sea-Level Change. *Science*, v. 310, n. 5752, p. 1293–1298, 25 nov. 2005.

MOORE, D. M.; REYNOLDS, R. C. *X-ray diffraction and the identification and analysis of clay minerals*. Oxford: Oxford University Press, 1997.

MORTON, O. Major shifts in climate and life may rest on feast of clay. *Science*, v. 309, n. 5739, p. 1329–1321, 2005.

MURRAY, H. H. *Applied clay mineralogy: Occurrences, processing and application of kaolins, bentonites and palygorskite-sepiolite, and common clays*. Oxford: Elsevier B.V., 2007.

ÖZCAN, E. et al. Biometric analysis of middle and upper Eocene Discocyclinidae and Orbitoclypeidae (Foraminifera) from Turkey and updated orthophragmine zonation in the Western Tethys. *Micropaleontology*, v. 52, n. 6, p. 485–520, 2006.

ÖZKUL, M.; KEREY, İ. E. Facies analysis on deep sea, shelf complex: Kırkgeçit Formation (Middle Eocene–Oligocene), Baskil-Elazığ. *Turkish Journal of Earth Sciences*, v. 5, p. 57–70, 1996.

PAK, D. K.; MILLER, K. G. Paleocene to Eocene benthic foraminiferal isotopes and assemblages: Implications for deepwater circulation. *Paleoceanography*, v. 7, n. 4, p. 405–422, 1992.

PALMER, M. R.; HELVACÍ, C.; FALLICK, A. E. Sulphur, sulphate oxygen and strontium isotope composition of Cenozoic Turkish evaporites. *Chemical Geology*, v. 209, n. 3–4, p. 341–356, 2004.

PANDARINATH, K. Clay minerals in SW Indian continental shelf sediment cores as indicators of provenance and palaeomonsoonal conditions: a statistical approach. *International Geology Review*, v. 51, n. 2, p. 145–165, 2009.

PASCHER, K. M. et al. Expansion and diversification of high-latitude radiolarian assemblages in the late Eocene linked to a cooling event in the Southwest Pacific. p. 2977–3018, 2015.

PAYROS, A. et al. Early Eocene climatic optimum : Environmental impact on the North Iberian continental margin. *GSA Bulletin* n. 11, p. 1632–1644, 2015.

PETSCHICK, R. *MacDiff 4.2.5., http://www.geologie.uni-frankfurt.de/staff/homepages/petschick/ petschick.html*, 2001.

PETSCHICK, R.; KUHN, G.; GINGELE, F. Clay mineral distribution in surface sediments of the South Atlantic: sources, transport, and relation to oceanography. *Marine Geology*, v. 130, p. 203–229, 1996.

PLETSCH, T. Origin of lower Eocene palygorskite clays on the Côte D'Ivoire-Ghana transfotm margin, eastern Equatorial Atlantic. *Proceedings of the Integrated Ocean Drilling Program,* v. 159, p. 141–156, 1998.

PLETSCH, T. Palaeoenvironmental implications of palygorskite clays in Eocene deep-water sediments from the western Central Atlantic. *Geological Society, London, Special Publications*, v. 183, n. 1, p. 307–316, 2001.

PRINS, M. A.; POSTMA, G. Effects of climate, sea level, and tectonics unraveled for last deglaciation turbidite records of the Arabian Sea. *Geology*, v. 28, n. 4, p. 375–378, 2000.

PUJALTE, V.; BACETA, J. I.; SCHMITZ, B. A massive input of coarse-grained siliciclastics in the Pyrenean Basin during the PETM: The missing ingredient in a coeval abrupt change in hydrological regime. *Climate of the Past*, v. 11, n. 12, p. 1653–1672, 2015.

RATEEV, M. et al. The Distribution of Clay Minerals in the Oceans. *Sedimentology*, v. 13, n. 1–2, p. 21–43, 1969.

RATEEV, M. A.; SADCHIKOVA, T. A.; SHABROVA, V. P. Clay minerals in recent sediments of the World Ocean and their relation to types of lithogenesis. *Lithology and Mineral Resources*, v. 43, n. 2, p. 125–135, 2008.

RODELLI, D.; JOVANE, D.; ÖZCAN, E.; GIORGIONI, M.; COCCIONI, R.; FRONTALINI, F.; SICILIANO, E. R.; BROGI, A.; CATANZARITI, A.; LESS, GY.; ROSTAMI, M.A. High-resolution integrated magnetobiostratigraphy of a new middle Eocene section from the western branch of the Neo-Tethys (Elazığ Basin, eastern Turkey). *Geological Society of America Bulletin. Accepted,* 2017.

ROBERT, C.; CHAMLEY, H. Development of early Eocene warm climates, as inferred from clay mineral variations in oceanic sediments. *Global and Planetary Change*, v. 3, n. 4, p. 315–331, 1991.

ROBERT, C.; KENNET, J. P. Antarctic subtropical humid episode at the Paleocene-Eocene boundary : Clay-mineral evidence. *Geology*, v. 22, p. 211–214, 1994.

SARRAZIN, P. et al. Field deployment of a portable xrd/xrf instrument on mars analog terrain. *Advances in X-ray analysis*, v. 48, 2005.

SAVIAN, J. F. et al. Enhanced primary productivity and magnetotactic bacterial production in response to middle Eocene warming in the Neo-Tethys Ocean. *Palaeogeography, Palaeoclimatology, Palaeoecology*, v. 414, p. 32–45, 2014.

SAVIAN, J. F. et al. Environmental magnetic implications of magnetofossil occurrence during the Middle Eocene Climatic Optimum (MECO) in pelagic sediments from the equatorial Indian Ocean. *Palaeogeography, Palaeoclimatology, Palaeoecology*, v. 441, n. October, p. 212–222, jan. 2015.

SCHULTE, P.; SCHEIBNER, C.; SPEIJER, R. P. Fluvial discharge and sea-level changes controlling black shale deposition during the Paleocene–Eocene Thermal Maximum in the Dababiya Quarry section, Egypt. *Chemical Geology*, v. 285, n. 1–4, p. 167–183, jun. 2011.

SEXTON, P. F. et al. Eocene global warming events driven by ventilation of oceanic dissolved organic carbon. *Nature*, v. 471, n. 7338, p. 349–352, 17 mar. 2011.

SHOVAL, S. Deposition of volcanogenic smectite along the southeastern Neo-Tethys margin during the oceanic convergence stage. *Applied Clay Science*, v. 24, n. 3–4, p. 299–311, 2004.

SINGER, A. The paleoclimatic interpretation of clay minerals in sediments — A review. *Earth-Science Reviews*, v. 21, p. 251–293, 1984.

SLUIJS, A. et al. A middle Eocene carbon cycle conundrum. *Nature Publishing Group*, v. 6, n. 6, p. 429–434, 2013.

SOLIMAN, M. F. et al. Enhanced coastal paleoproductivity and nutrient supply in Upper Egypt during the Paleocene/Eocene Thermal Maximum (PETM): Mineralogical and geochemical evidence. *Palaeogeography, Palaeoclimatology, Palaeoecology*, v. 310, n. 3–4, p. 365–377, 2011.

SPOFFORTH, D. J. A. et al. Organic carbon burial following the middle Eocene climatic optimum in the central western Tethys. *Paleoceanography*, v. 25, n. 3, p. PA3210, 24 ago. 2010.

STEIN, R. *Clay Minerals*, 2016. (Nota técnica).

THIRY, M. Palaeoclimatic interpretation of clay minerals in marine deposits: an outlook from the continental origin. *Earth-Science Reviews*, v. 49, n. 1–4, p. 201–221, mar. 2000.

THIRY, M.; DUPUIS, C. Use of clay minerals for paleoclimatic reconstructions : Limits of the

method with special reference to the Paleocene-lower Eocene interval. *GFF*, v. 122, p. 166–167, 2000.

THIRY, M.; JACQUIN, T. Clay Mineral Distribution Related to Rift Activity, Sea-Level Changes and Paleoceanography in the Cretaceous of the Atlantic Ocean. *Clay Minerals*, v. 28, n. 1, p. 61–84, 1993.

THIRY, M.; PLETSCH, T. Palygorskite Clays in Marine Sediments: Records of Extreme Climate. In: *Developments in Clay Science*. [s.l: s.n.]. v. 3p. 101–124.

TURAN, M.; BINGÖL, A. F. Tectono-stratigraphic characteristics of the region between Kovancılar–Baskil (east of Elazığ, E. Turkey). *Proceedings of Ahmet Acar Symposium, Çukurova University, Adana–Turkey*, p. 193–204, 1991.

VELDE, B. *Origin and mineralogy of clays: clays and the environment*. Berlin: Springer-Verlag, 1995.

VENKATARATHNAM, K.; BISCAYE, P. E. Clay mineralogy and sedimentation in the eastern Indian Ocean. *Deep Sea Research and Oceanographic Abstracts*, v. 20, p. 727–738, 1973.

WANG, C. et al. The Eocene–Oligocene climate transition in the Tarim Basin, Northwest China: Evidence from clay mineralogy. *Applied Clay Science*, v. 74, n. October, p. 10–19, abr. 2013a.

WANG, C. W. et al. The early-Eocene climate optimum (EECO) event in the Qaidam basin, northwest China: clay evidence. *Clay Minerals*, v. 46, n. 4, p. 649–661, 1 dez. 2011.

WANG, X. et al. Cenozoic paleo-environmental evolution of the Pamir – Tien Shan convergence zone. *Journal of Asian Earth Sciences*, v. 80, n. December, 2013b.

WESTERHOLD, T. et al. On the duration of magnetochrons C24r and C25n and the timing of early Eocene global warming events: Implications from the Ocean Drilling Program Leg 208 Walvis Ridge depth transect. *Paleoceanography*, v. 22, p. 1–19, 2007.

WESTERHOLD, T.; RÖHL, U.; LASKAR, J. Time scale controversy: Accurate orbital calibration of the early Paleogene. *Geochemistry, Geophysics, Geosystems*, v. 13, n. 6, p. 1–19, 2012.

WILSON, M. J. The origin and formation of clay minerals in soils " past , present and future perspectives. *Clay Minerals*, v. 34, p. 7–25, 1998.

WINDOM, H. L. Lithogeneous material in marine sediments. In: RILEY, J. P.; CHESTER, R. (Eds.). . *Chemical Oceanography*. New York/London: [s.n.]. p. 103–155.

X. GINGELE, F. et al. History of the South Java Current over the past 80 ka. *Palaeogeography,*

Palaeoclimatology, Palaeoecology, v. 183, n. 3–4, p. 247–260, 2002.

YALÇIN, H.; BOZKAYA, Ö. Sepiolite-palygorskite from the Hekimhan region (Turkey). *Clays and Clay Minerals*, v. 43, n. 6, p. 705–717, 1995.

YALÇIN, H.; BOZKAYA, Ö. Sepiolite-palygorskite occurrences in Turkey. *Developments in Clay Science*, v. 3, p. 175–200, 2011.

ZACHOS, J. et al. Trends , Rhythms , and Aberrations in Global Climate 65 Ma to Present. v. 292, n. April, p. 686–694, *Science*, 2001.

ZACHOS, J. C. et al. Rapid acidification of the ocean during the Paleocene-Eocene thermal maximum. *Science*, v. 308, n. 5728, p. 1611–1615, 2005.

ZACHOS, J. C.; DICKENS, G. R.; ZEEBE, R. E. An early Cenozoic perspective on greenhouse warming and carbon-cycle dynamics. *Nature*, v. 451, n. 7176, p. 279–283, 17 jan. 2008.

ZHANG, C.; GUO, Z. Clay mineral changes across the Eocene-Oligocene transition in the sedimentary sequence at Xining occurred prior to global cooling. *Palaeogeography, Palaeoclimatology, Palaeoecology*, v. 411, n. July, p. 18–29, 2014.

ZHOU, C. H.; KEELING, J. Fundamental and applied research on clay minerals: From climate and environment to nanotechnology. *Applied Clay Science*, v. 74, p. 3–9, 2013.

Supplementary material

	Carbonates		***Quartz***	***Plagioclase***	***K-Feldspar***	***Phyllosilicates***
depth (m)	Calcite	Dolomite	Quartz	Albite	Orthoclase	
357	73.398	6.373	7.658	2.312	0.000	10.259
353	68.618	6.725	8.443	2.439	0.000	13.775
348	52.589	9.033	10.540	5.197	2.822	19.819
342	55.485	6.726	10.927	4.573	0.000	22.289
336	52.80381242	10.10167474	8.541447643	3.749722004	3.193696054	21.6096472
332	52.57479554	4.920957578	10.66715184	4.406839048	3.618679653	23.81872711
329	60.34671509	5.368293407	7.389958177	1.497920912	6.243644465	19.1534679
326	58.77376169	5.117460309	10.60660716	4.33452557	2.10190787	19.06573737
323	56.2420042	5.293537462	10.33219159	4.02395204	2.080205914	22.0281088
321	78.194	2.607	7.052	2.429	0.000	9.718
319	79.311	2.204	6.743	2.130	0.000	9.613
313	79.857	3.068	6.640	1.430	0.000	9.005
309	49.18732394	5.55302781	12.30716064	6.681046249	2.466728881	23.80471242

305	70.812	3.671	8.779	1.925	0.000	14.813
303	74.362	2.618	7.879	2.021	0.000	13.119
298	72.118	4.017	8.458	2.767	0.736	11.904
296	62.3460970	3.6976181	10.7973426	4.2852618	0.9995722	17.8741084
293	75.237	2.341	7.371	2.520	1.523	11.008
289	75.480	2.528	7.022	2.198	0.000	12.771
285	80.48847046	1.048465526	7.800241433	1.29559681	0	9.367225765
280	77.95704641	1.156347777	6.757560609	1.587382082	0	12.54166314
274	82.33126497	0.580931537	6.826308993	1.10544317	0	9.156051336
271	78.9877094	0.649952047	7.730782352	1.489451655	0	11.14210454
264	85.95396143	0.512003986	4.059206793	0.764781096	0	8.71004667
261.5	83.3537914	0.888040171	5.283648367	1.166374736	0	9.308145338
259	82.64257634	1.058362094	6.112226991	1.574293899	0	8.612540674
256	79.59900642	1.269374603	7.038272334	1.626979462	0	10.4663672
252	78.62764195	0	8.31579348	2.787903116	0	10.26866147
248	74.458	1.126	8.135	3.352	0.000	12.930
246	76.85063998	0.863344223	8.344510846	2.676626548	0	11.26487844
243	76.71349537	1.91341539	7.226109138	2.345441287	0	11.8015388
240	75.6866233	1.312649867	8.242220093	2.104957556	0	12.65354916
236	67.92599541	1.465446847	9.786473035	6.034005582	0	14.78807912
233	86.26937492	0	6.498653202	0.988327088	0	6.243644779
230	74.09695197	0.343435024	9.4354254	2.701962728	0	13.42222486
228	66.75867245	1.567021049	9.850317016	3.3707185	0.897291348	17.55597968
224	63.38009283	1.703906557	11.56151284	5.274044814	0	18.08044295
220	56.39390974	2.484323799	13.13101604	4.996719652	1.214428829	21.77960189
216	73.93996433	2.099662585	9.298869983	2.452013544	0	12.20948956
212	63.33809612	1.825230832	11.85340931	3.967899855	0	19.01536388
210	70.51009297	0.708015935	9.934456233	2.39695178	1.408579071	15.04190397
206	68.331	1.398	10.350	2.716	0.489	16.716
201.5	66.48260747	1.030373109	8.438003423	3.99636038	0.879806046	19.17284959
194	61.26779076	0.283128249	11.45871015	3.592495448	0	23.39787541
192	49.50639765	0.60012783	14.63439911	6.576741988	1.696527733	26.98580565
188	63.13994239	0.348026389	11.81393374	3.382871086	0	21.31522645
186	61.2129136	0.843515639	10.096082	5.162034015	0	22.68545479
183	52.67278721	2.041201143	13.34972465	5.047630638	0	26.88865641
180	49.46607099	0.295404564	13.3870036	4.598558611	1.933811563	30.31915074
176	55.75522037	1.387916423	13.08206135	4.942898104	1.404125666	23.42777809
174	45.26490434	3.334608376	15.39523865	5.279392152	1.721409441	29.00444703
170	47.23850928	1.801070506	15.36633896	5.005642903	0	30.5884383
169	50.35000628	0.846642224	14.93970681	7.897684314	2.728664305	23.23729606
167	54.33400055	0.525210729	14.6754793	5.188121235	0	25.27718815
163	47.09736935	3.466896473	14.38349359	5.175696489	0.695165813	29.18137836
159	44.38629546	2.61354363	14.58084616	7.949372639	0	30.46994203

154	54.16621076	2.036135045	12.3136819	4.372398875	1.504381392	25.60719209
150	47.08442218	1.987355902	14.03925631	4.281617617	0.883351641	31.72399643
145	44.88285879	3.039174042	13.87851152	5.271356793	3.294169131	29.63392968
143	56.26788075	2.301371354	12.37619347	4.000363081	0	25.05419131
139	63.10071303	2.340819651	11.24613754	3.001039419	0	20.31129032
137	52.91109435	2.425567211	16.81787484	3.832062359	0	24.01340121
134	58.83812216	1.651120144	11.65446644	3.434533428	0	24.42175786
132	54.34009073	3.174434052	13.15470427	4.342456181	0.970523394	24.01779143
128	58.45281513	2.140122403	10.93723017	3.22954	0.837268295	24.40302406
126	64.37365131	1.693496976	8.984493817	2.628947593	0.947797546	21.37161276
124	66.04967799	1.951635451	8.657250541	3.230234505	1.356392309	18.75480924
122	56.33738775	3.268176782	11.84694565	4.346307462	3.609313227	20.59186914
120	56.93697712	2.269000333	13.57821037	4.857501528	0	22.35831069
118	56.8123404	3.813970241	19.83538981	4.397675354	0.805491883	14.33513226
113	53.47781155	1.749915782	10.66419967	5.978011814	4.769375995	23.36068516
110	78.365	1.196	7.068	2.742	0.995	9.634
106	80.981	0.727	8.318	1.271	0.000	8.703
103	72.688	1.420	10.849	2.121	0.000	12.922
100	75.971	1.560	9.128	2.237	0.000	11.104
94	83.614	0.754	7.929	0.725	0.000	6.978
90	60.54171006	3.804898048	13.81675419	4.9030601	0	16.93357757
88	69.78928562	2.877023869	10.33842799	2.591810948	0	14.40345162
86	47.153	3.164	12.741	6.769	4.866	25.307
84	66.60659851	2.665803235	11.5595614	4.171999506	0	14.99603735
82	69.29915535	2.652461701	9.974813623	3.379672724	0	14.69389656
80	59.15958015	4.518496834	12.75777293	5.203521175	0	18.36062888
79	58.56686319	7.380463208	13.69764921	5.775637824	0	14.57938662
77	73.152	2.303045831	8.515455746	3.360237593	0	12.66947366
76	70.31608163	4.134700793	7.567083265	3.707488446	0.630389991	13.64425592
73	60.5906086	7.534697529	11.02747335	4.331913545	3.11389114	13.40141585
66	73.28899545	2.350568037	8.468162664	3.815511768	0	12.07676205
63	68.18898367	4.406142685	10.89911603	3.248102426	0	13.25765523
60	60.75154015	4.441593459	12.70050662	5.147504689	1.525050621	15.43380451
57	53.329	3.715	12.391	6.422	0.000	24.143
54	77.48976619	1.996189534	7.065622855	3.328432422	0	10.11998897
50	73.91531627	1.967653094	9.061385768	3.55107635	1.129613352	10.37495515
47	45.927	3.662	14.405	6.577	5.951	23.479
45	51.773	6.280	14.767	7.009	1.482	18.690
42	64.51831364	3.89391192	11.0023584	7.340377961	0	13.24503804
38	60.97835822	5.272768417	13.48993123	5.726094051	0	14.53284809
34	65.40101414	4.44869993	10.66430894	5.131893133	2.167152394	12.1869315
29	59.09640167	6.114590823	13.85034551	5.377593881	0	15.56106807
27	59.66845791	6.675911884	12.38111736	6.652065833	0	14.62244696

24	66.22440388	4.484962177	10.16223905	4.563604539	0	14.56479031
19	44.8218	5.6833	14.8738	5.8543	0.0000	28.7668
16	58.78319326	4.261576295	14.33146945	8.494801337	0	14.12896027
13	65.98483679	3.959108004	10.87495696	7.149258689	0	12.03183955
11	66.33404327	4.517687941	11.18671737	4.672872365	0	13.28867907
8	55.19766433	4.703998598	15.89228792	6.708784117	0	17.49726506
4	54.86338001	7.309355514	14.63930787	7.799074531	0	15.38888208
0	60.33965741	10.62354503	11.25508546	4.138075927	0	13.6436366

Table 2: Percentages of bulk mineralogy along the Baskil section

depth (m)	***Smectite***	***Palygorskite***	***Illite***	***Chlorite + Kaolinite***	***Chlorite***	***Kaolinite***
353	60.60331734	9.916940189	22.21289408	7.266848397	5.018687837	2.24816056
342	49.920056	11.17300324	30.68449749	8.222443266	5.351440159	2.871003107
332	46.68252986	11.27136931	34.29460373	7.751497106	5.161039526	2.59045758
319	48.51344259	14.72031875	28.15588524	8.610353418	5.543022714	3.067330704
309	73.12695538	6.129393961	14.08890248	6.654748183	4.295073281	2.359674902
303	78.75889714	3.967703586	10.94404902	6.329350261	4.469296307	1.860053954
296	62.21753667	8.702864532	21.17074194	7.908856867	4.852674168	3.056182699
285	80.00659623	3.72163905	9.799724778	6.472039941	4.47957124	1.992468701
280	84.87950429	3.229243467	5.545090843	6.346161402	3.919856231	2.426305171
274	84.75503966	1.888102646	8.404154665	4.952703029	3.085612601	1.867090427
264	77.12912601	3.838120908	11.84721386	7.185539223	4.665416699	2.520122524
259	83.39053025	2.800670881	7.77396465	6.034834215	4.739728214	1.295106001
256	79.70298407	2.807457724	10.90357151	6.585986688	4.511046796	2.074939892
248	83.28340758	2.79758905	8.305279497	5.61372387	3.183128481	2.430595389
246	79.61908829	1.396483279	14.70450935	4.279919084	2.959096374	1.320822711
240	78.50873566	4.272717874	9.955546366	7.263000103	4.216439657	3.046560446
233	75.97541798	3.492815183	12.26064166	8.271125169	5.312655741	2.958469429
228	81.51757707	2.584369701	8.548098838	7.349954395	4.880977466	2.468976928
224	82.63000456	2.010686259	8.473606377	6.885702809	4.272202249	2.61350056
220	71.79654006	0	21.24746739	6.955992549	4.055736519	2.900256029
216	65.84668556	7.283887468	19.7768715	7.092555471	5.091190808	2.001364663
210	79.38440555	2.843676593	10.6933394	7.078578465	5.353683483	1.724894982
206	83.37207767	1.378084019	10.83549059	4.414347716	3.172648001	1.241699715
201.5	83.79752301	1.856431595	9.524557237	4.821488155	3.610898055	1.210590099
195	76.88133475	1.900643629	16.22895707	4.98906455	3.255015605	1.734048945
192	79.30444928	2.945780314	11.38457451	6.365195894	4.487506172	1.877689723
190	78.59086276	3.364194456	13.43608452	4.608858266	2.878703625	1.730154641
185	70.39491392	3.172352613	19.9985594	6.434174062	4.46494219	1.969231873

180	70.84321146	3.986741036	16.33835358	8.831693923	5.802817451	3.028876473
176	71.23467854	5.603522948	15.45032434	7.711474176	4.592036736	3.11943744
170	69.66876317	5.984779867	17.38041022	6.966046744	4.416617265	2.549429478
167	78.70063826	5.859841371	9.890095706	5.549424664	3.554173506	1.995251158
163	69.79748419	4.013961369	20.33270164	5.855852801	3.881052943	1.974799858
159	84.94302912	3.488049235	6.791672292	4.77724935	2.592710857	2.184538493
154	79.76002052	3.699087775	11.70597397	4.834917729	2.9003153	1.934602429
150	82.04762744	4.072161443	9.104143912	4.776067204	3.664113413	1.111953791
147	74.50178504	1.771529937	20.34513215	3.381552872	1.828884412	1.55266846
145	83.73009217	2.278806766	10.1913977	3.799703369	2.815442858	0.984260511
143	81.35998059	2.582086409	12.6619802	3.395952794	2.165490975	1.23046182
139	85.62210098	0	10.78926182	3.588637198	2.521396486	1.067240712
137	82.6829006	1.367497277	12.01152644	3.938075688	2.28479883	1.653276859
134	79.985	0.000	15.981	4.034	2.318867106	1.714655254
130	84.36414574	0	11.7011261	3.934728164	2.662679059	1.272049105
128	78.217	0.000	16.798	4.985	3.432229149	1.552493894
126	83.45203559	0	12.89496371	3.653000705	2.272107677	1.380893028
124	80.12306335	0	15.75789882	4.119037827	2.831438133	1.287599694
122	78.60235735	3.920839234	12.7361754	4.740628016	3.024193735	1.716434282
113	70.9612611	0	22.15295078	6.885788122	5.242083861	1.643704261
106	68.87434033	0	25.21984367	5.905815995	4.032347724	1.873468271
100	69.18284271	0	23.18669093	7.630466367	5.815452523	1.815013845
90	64.165	0.000	29.336	6.499	4.437464302	2.061571957
86	81.590	0.000	14.149	4.260	3.218381975	1.042066393
82	64.15296565	0	26.77025922	9.076775131	6.552429153	2.524345978
80	58.10181545	0	33.5191927	8.378991844	5.656063923	2.722927921
76	58.61368641	0	32.75707586	8.629237738	6.861185062	1.768052676
73	63.82349056	0	29.60220762	6.57430182	5.47997712	1.094324699
66	56.37093188	0	34.46435774	9.164710384	7.891833942	1.272876442
60	57.87810023	0	34.49970049	7.622199285	6.300286451	1.321912834
50	55.74810772	0	35.3300036	8.921888677	6.653875189	2.268013488
47	70.07113392	4.151381726	19.33869775	6.438786603	4.990232889	1.448553714
42	55.22506028	0	36.254161	8.520778723	6.759387852	1.761390871
38	36.068	0.000	52.672	11.260	8.546579653	2.713447897
35	47.97400416	0	43.70783903	8.318156803	6.327946538	1.990210265
29	53.78341242	0	37.27119484	8.945392733	7.54041904	1.404973694
27	56.38445309	0	34.0714463	9.544100612	7.502361931	2.041738681
24	36.444	0.000	51.585	11.971	9.025049507	2.94571115
19	58.69290002	0	32.41139294	8.895707044	6.503775573	2.391931472
16	55.3407753	0	35.18686876	9.472355942	7.699646607	1.772709335
8	50.18350603	0	41.31857803	8.49791594	7.512068474	0.985847466

Mean	74.50178504	1.900643629	16.22895707	6.585986688	4.657934861	1.965702441
Staadard deviation	12.75909661	3.139839529	11.37820572	1.948280457	1.682556649	0.608609097

Table 3: Percentages of clay mineralogy along the Baskil section

depth (m)	*initial weight/mass (g)*	*empty bottle and lid (g)*	*bottle, lid and dried sample (g)*	*weight/mass loss (total) (g)*	*weight % loss*
353	10.004	49.455	58.613	-0.846	8%
342	15.062	49.279	63.314	-1.027	7%
332	9.59	49.657	58.123	-1.124	12%
319	11.323	49.903	60.506	-0.72	6%
309	9.611	49.855	58.616	-0.85	9%
303	13.884	49.172	62.14	-0.916	7%
296	9.131	49.205	57.251	-1.085	12%
285	12.854	49.457	61.107	-1.204	9%
274	12.146	49.28	60.405	-1.021	8%
264	14.098	49.146	62.174	-1.07	8%
256	10.559	49.79	59.374	-0.975	9%
246	15.883	49.346	64.28	-0.949	6%
233	11.463	49.487	59.973	-0.977	9%
224	12.491	49.356	60.961	-0.886	7%
216	8.462	49.848	57.305	-1.005	12%
210	12.815	49.603	61.346	-1.072	8%
206	9.116	49.786	57.983	-0.919	10%
201.5	10.906	49.322	59.219	-1.009	9%
195	7.987	49.246	56.478	-0.755	9%
192	10.709	49.169	59.12	-0.758	7%
190	6.959	49.813	56.005	-0.767	11%
185	6.749	49.386	55.199	-0.936	14%
180	8.961	49.514	57.67	-0.805	9%
176	10.991	49.84	59.972	-0.859	8%
170	13.449	49.777	61.9	-1.326	10%
167	6.614	49.512	55.383	-0.743	11%
163	22.736	49.5	67.896	-4.34	19%
159	14.776	49.273	62.491	-1.558	11%
154	10.389	49.809	58.857	-1.341	13%
150	12.621	49.338	60.32	-1.639	13%

147	14.373	49.133	61.292	-2.214	15%
145	12.413	49.453	60.229	-1.637	13%
143	11.092	49.781	58.822	-2.051	18%
139	8.984	49.337	56.371	-1.95	22%
137	8.281	49.476	56.201	-1.556	19%
132	19.95	49.576	65.119	-4.407	22%
128	10.208	49.141	57.805	-1.544	15%
126	12.453	49.466	60.995	-0.924	7%
124	9.615	49.581	58.275	-0.921	10%
123	11.77	49.348	59.701	-1.417	12%
122	5.548	49.341	53.937	-0.952	17%
120	9.214	49.593	57.293	-1.514	16%
113	19.565	49.843	67.446	-1.962	10%
100	15.036	49.477	62.638	-1.875	12%
90	9.145	49.162	56.664	-1.643	18%
86	7.93	49.27	55.894	-1.306	16%
82	10.557	49.14	58.436	-1.261	12%
80	7.618	49.835	57.07	-0.383	5%
76	7.643	49.45	56.091	-1.002	13%
73	11.316	49.665	58.883	-2.098	19%
66	12.875	49.39	58.889	-3.376	26%
60	5.333	49.163	53.522	-0.974	18%
50	9.44	49.333	57.294	-1.479	16%
45.5	14.817	49.346	60.17	-3.993	27%
42	8.724	49.605	56.971	-1.358	16%
35	10.272	49.851	59.278	-0.845	8%
27	5.32	49.586	54.813	-0.093	2%
13	7.023	49.774	56.427	-0.37	5%
8	8.007	49.475	56.885	-0.597	7%

Table 4: Weight loss after the removal of organic matter and calcium carbonate combined during the initial steps for clay minerology sample preparation.

Depth (m)	*SiO2*	*TiO2*	*Al2O3*	*Fe2O3*	*MnO*	*MgO*	*CaO*	*Na2O*	*K2O*	*P2O5*
239	14.33	0.185	3.18	2.14	0.055	1.26	42.01	0.02	0.6	0.049
213	20.21	0.258	4.27	3.14	0.068	1.61	36.99	0.17	0.82	0.109
206	22	0.289	4.93	2.82	0.064	1.87	35.15	0.18	0.94	0.076
204	18.59	0.281	4.66	2.54	0.054	1.73	38.25	0.13	0.91	0.087
200.5	41.67	0.414	6.21	2.81	0.032	1.3	22.95	1.02	1.04	0.050
192	25.85	0.334	5.82	3.01	0.024	1.61	33.86	0.21	1.02	0.058
188	26.46	0.404	7.11	3.26	0.033	2.02	30.37	0.24	1.28	0.062
178	26.59	0.377	6.45	3.23	0.034	1.83	31.99	0.27	1.16	0.073

162	27.14	0.428	7.29	3.6	0.033	2.51	29.59	1.14	1.38	0.059

Table 5: Experimental inorganic geochemistry tested in a few samples using X-ray Fluorescence (XRF) performed at the Institute of Geosciences (IGc).

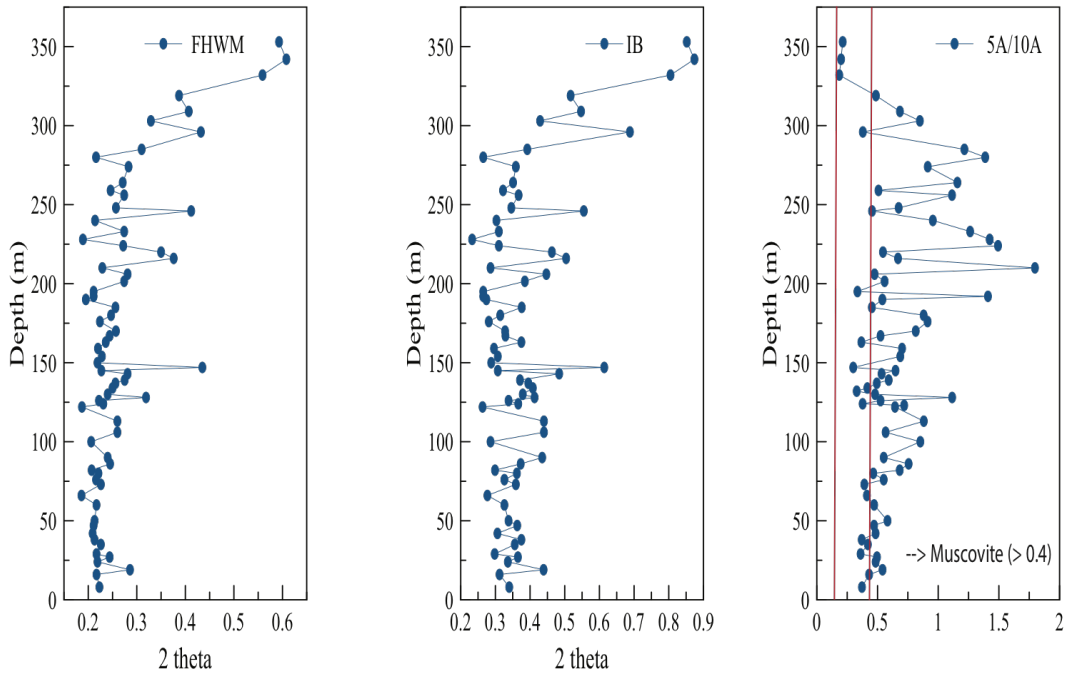

Figure 23: Illite crystallinity shown by full width half maximum (FWHM) and integral breadth (IB) presenting the same pattern. Illite chemistry (Esquivin, 1969) showing that illite was probably altered from muscovite and ratios of 5A/10A peak area ratios indicate greater values for almost the entire section. Exceptions are made only in the last few meters.

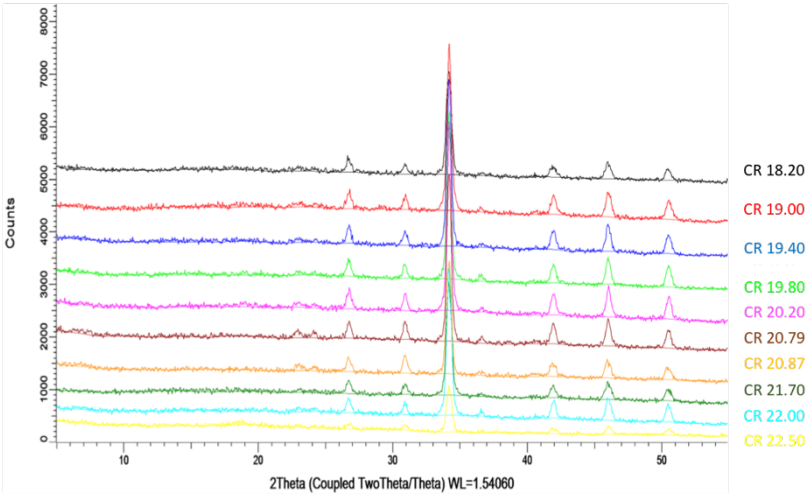

Figure 24: Samples from the Contessa Road, Italy (upper Paleocene) analyzed through the BTX.

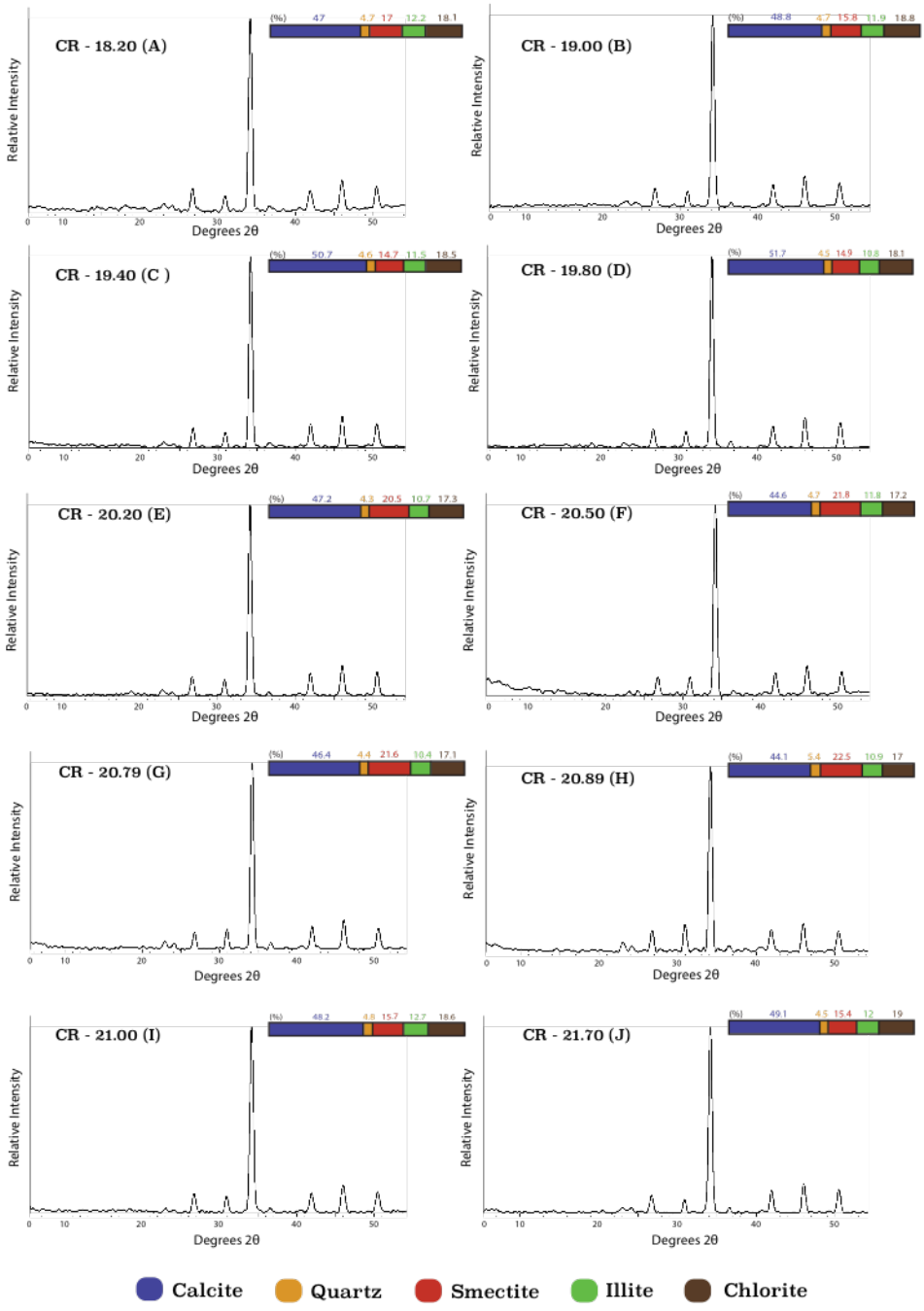

Figure 25:Semi-quantification based on HighScore sorftware, on the same Contessa Road samples.

Preparation of Samples for X-ray Diffraction Analysis of Clay Minerals

General

Use distilled or deionized water for mixing chemicals and in all steps of this procedure.
Number samples, beakers, test tubes and corresponding slots on centrifuge.
Always balance test tubes in centrifuge.

Chemicals Needed

Morgan's Solution – 82 g sodium acetate plus 27 ml glacial acetic acid, diluted to 1 liter.

30% Hydrogen Peroxide (H_2O_2)

2% Sodium Carbonate – 20 g Na_2CO_3, diluted to 1 liter

0.01% Sodium Carbonate – 0.1 g Na_2CO_3 diluted to 1 liter OR Use 5 ml of the 2% Na_2CO_3, add to 1 liter of water

1 M Magnesium Chloride Hexahydrate ($MgCl_2 \cdot 6H_2O$) – 203.3 g $MgCl_2 \cdot 6H_2O$ diluted to 1 liter

Ethylene Glycol

If testing for vermiculite (Ba-saturation): 1 M Ba Cl_2 – 244.3 g $BaCl_2$, diluted to 1 liter

Equipment Needed

Beakers – (1) 250 ml and (1) 1000 ml or larger per sample

Test tubes – (1) 50 ml plastic tube per sample

Squirt bottles – Five total: (1) Morgan's Solution; (1) 2% Na_2CO_3; (1) 0.01% Na_2CO_3; (1) $MgCl_2$; and (1) distilled water

Magnetic stirrer and magnets

Desiccator – be sure the desiccant is fresh (i.e. dry, the blue indicator should not be purple) and the lids are greased. If desiccant is purple (saturated), see "Desiccant in desiccator" procedure

CLAY MINERALOGY PROCEDURE

1. Remove organic matter (OM) and $CaCO_3$ from sample by adding the following chemicals per 10 cc of sediment:

- 50 ml water
- 20 ml H_2O_2
- 20 ml Morgan's Solution

Stir and let sit for 4 to 5 days (depending on the amount of OM and $CaCO_3$

If a lot of organic matter or $CaCO_3$ is present, the mixture will bubble. If a vigorous reaction is observed, double the amount of Hydrogen Peroxide and Morgan's solution after the reaction has quieted. If it still reacts after several hours, add more H_2O_2 and Morgan's Solution (always together as the Morgan's Solution acts as a buffer) in increments of 10 ml each every 3 hours until reaction is complete.

2. After 2 days, transfer sample solution to centrifuge tube in the following manner:

• fill test-tube with sample solution, centrifuge 5 min. @ 1000-1500 rpm
• pour off clear liquid and add more solution
• when all of the sample is concentrated at the bottom of the tube and the last of the liquid is discarded, then <u>wash</u> the sample
• use a squeeze bottle to squirt Morgan's Solution hard enough to suspend all sediment (or stir with plastic stirrer making sure to wash the sediment off the stirrer back into the test tube)
• centrifuge for 5 minutes @ 1000-1500 rpm and pour off liquid
• do this **twice**

3. Wash sample into a beaker using 50 ml 2% Na_2CO_3

• cover with a watch glass and stir with magnetic stirrer for 5 min. at the highest speed magnet will allow (the highest speed at which the vortex created is preserved)
• re-concentrate all sample in test tube (as above) using 0.01% Na_2CO_3 to rinse residue in beaker into tube

4. Thoroughly suspend sediment in tubes with 0.01% Na_2CO_3

• centrifuge for 3 min. at 850 rpm (set time so that the centrifuge spins for 3 min at 850 rpm, it may take 25 sec to get to 850 rpm);
• all material still in suspension has a settling diameter of 2 μm or less
• pour off suspension into large beaker and **save**
• the sediment is again suspended (using 0.01% Na_2CO_3), centrifuged again, and the supernatant is poured into the same appropriate large beaker
• begin with different tube from centrifuge each time you suspend the clay, because the sediment settles slightly while you re-suspend the other samples
• repeat until supernatant is clear
• if after 10 runs the supernatant isn't clear, it probably contains colloidal material, so stop
• save silt and sand concentrated in the test tube in a plastic bottle and put aside
• wash out test tube
• concentrate (as in #2) the suspended clay (from large beaker) back into test tube

5. Mg saturate the clay by washing (as in #2) 4 times with $MgCl_2$ (1000-1500 rpm for 5 min.); discard the liquid

6. Remove excess salts by washing clay (as in #2) 2 times with distilled water (1000-1500 rpm for 5 min.); discard the liquid

7. Spread clay evenly over a plastic or glass insert in the aluminum holder, layer should be nearly translucent when held up to the light

8. Glycolate slides:
- place aluminum holder with clay on a "holy" plate or screen over a bowl of ethylene glycol
- put this in an oven at 65°C for 1-4 hours
- remove from oven and place glycol/holy plate/sample set up in a dessicator for 18-24 hours. This expands the smectite lattice so that smectite can be distinguished from chlorite and vermiculite.

9. Samples are now ready to x-ray using the Clay Min program in the XRD data collector, which will run the samples from 3°-35° 2Ø at 40 kV and 45 mA and again from 24°-26° 2Ø at a slower speed

10. After step #7, if vermiculite is suspected (6.2° 2ø peak is greater than the 12.4° 2ø peak), take a split of the clay sample (before glycolation) for Ba-saturation
- follow through steps #5 and #6, using $BaCl_2$ instead of $MgCl_2$
- x-ray Ba-saturated slide, DON'T GLYCOLATE